Molecular Cell

Article

RNA interacts with topoisomerase I to adjust DNA topology

Graphical abstract

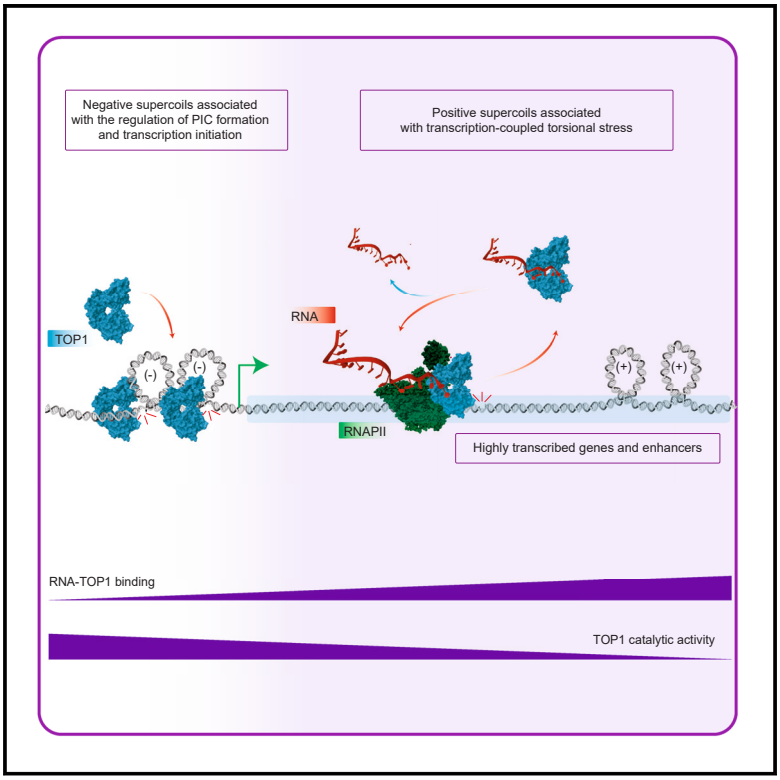

Authors

Mannan Bhola, Kouki Abe, Paola Orozco, ..., Eric L. Van Nostrand, Alfonso Mondragón, Shannon M. Lauberth

Correspondence

shannon.lauberth@northwestern.edu

In brief

Bhola and Abe et al. find that RNA acts as a regulatory switch that through TOP1-RNA interactions leads to significantly reduced levels of catalytically engaged TOP1 across the bodies of active genes. This RNA-based mechanism has important implications for the proper tuning of TOP1 relaxation of transcription-generated supercoils.

Highlights

- TOP1 activity levels are differentially enriched across protein-coding genes
- TOP1 is an RBP that predominantly binds mRNAs
- RNAs inhibit TOP1 activity at the single-molecule level
- Transcription-coupled topological stress is regulated by TOP1-RNA interactions

Bhola et al., 2024, Molecular Cell *84*, 1–17
September 5, 2024 Published by Elsevier Inc.
https://doi.org/10.1016/j.molcel.2024.07.032

CellPress

Molecular Cell

CellPress

Article

RNA interacts with topoisomerase I to adjust DNA topology

Mannan Bhola,[1,2,8] Kouki Abe,[1,2,8] Paola Orozco,[3] Homa Rahnamoun,[3] Pedro Avila-Lopez,[1,2] Elijah Taylor,[4] Nefertiti Muhammad,[1,2] Bei Liu,[6] Prachi Patel,[1,2] John F. Marko,[4] Anne C. Starner,[5] Chuan He,[6,7] Eric L. Van Nostrand,[5] Alfonso Mondragón,[4] and Shannon M. Lauberth[1,2,9,*]

[1]Simpson Querrey Institute for Epigenetics, Feinberg School of Medicine, Northwestern University, Chicago, IL 60611, USA
[2]Department of Biochemistry and Molecular Genetics, Feinberg School of Medicine, Northwestern University, Chicago, IL 60611, USA
[3]Section of Molecular Biology, University of California, San Diego, 9500 Gilman Drive, La Jolla, CA 92093, USA
[4]Department of Molecular Biosciences, Northwestern University, Evanston, IL 60208-3108, USA
[5]Verna & Marrs McLean Department of Biochemistry & Molecular Pharmacology and Therapeutic Innovation Center, Baylor College of Medicine, Houston, TX, USA
[6]Department of Chemistry, Department of Biochemistry and Molecular Biology, Institute for Biophysical Dynamics, The University of Chicago, Chicago, IL 60637, USA
[7]Howard Hughes Medical Institute, The University of Chicago, Chicago, IL 60637, USA
[8]These authors contributed equally
[9]Lead contact
*Correspondence: shannon.lauberth@northwestern.edu
https://doi.org/10.1016/j.molcel.2024.07.032

SUMMARY

Topoisomerase I (TOP1) is an essential enzyme that relaxes DNA to prevent and dissipate torsional stress during transcription. However, the mechanisms underlying the regulation of TOP1 activity remain elusive. Using enhanced cross-linking and immunoprecipitation (eCLIP) and ultraviolet-cross-linked RNA immunoprecipitation followed by total RNA sequencing (UV-RIP-seq) in human colon cancer cells along with RNA electrophoretic mobility shift assays (EMSAs), biolayer interferometry (BLI), and *in vitro* RNA-binding assays, we identify TOP1 as an RNA-binding protein (RBP). We show that TOP1 directly binds RNA *in vitro* and in cells and that most RNAs bound by TOP1 are mRNAs. Using a TOP1 RNA-binding mutant and topoisomerase cleavage complex sequencing (TOP1cc-seq) to map TOP1 catalytic activity, we reveal that RNA opposes TOP1 activity as RNA polymerase II (RNAPII) commences transcription of active genes. We further demonstrate the inhibitory role of RNA in regulating TOP1 activity by employing DNA supercoiling assays and magnetic tweezers. These findings provide insight into the coordinated actions of RNA and TOP1 in regulating DNA topological stress intrinsic to RNAPII-dependent transcription.

INTRODUCTION

Topoisomerase I (TOP1) supports RNA polymerase II (RNAPII)-dependent transcription through contributions to preinitiation complex (PIC) formation[1–6] and transcriptional elongation.[7] In the "twin domain model," as DNA moves through the transcription machinery, positive supercoils are driven in front and negative supercoils trail behind RNAPII.[8] While positive supercoils can promote and block RNAPII elongation,[9,10] negative supercoils support DNA melting and favor initiation.[11,12] The mechanisms underlying the regulation of TOP1 in dissipating positive and negative supercoils to facilitate transcription initiation and elongation, respectively, remain to be determined. Moreover, TOP1 is overexpressed in multiple cancers.[13–15] TOP1 activity is also stimulated by oncogenes, including mutant p53[16] and MYC,[17] to dissipate increased torsional stress associated with high levels of transcription that sustain cancer cell growth. Although there are clear links between TOP1 activity and oncogene-induced transcription, the requirement for TOP1 activity at specific target enhancers and gene loci in cancer cells remains to be elucidated.

TOP1 removes torsional stress by cleaving and resealing single-stranded DNA (ssDNA). During these cleavage and religation cycles, TOP1 forms a covalent bond with the DNA phosphodiester backbone giving rise to the formation of topoisomerase cleavage complexes (TOP1cc).[18,19] The formation of TOP1ccs is transient to avoid TOP1cc stabilization, which can lead to unresolved positive supercoils, obstacles for RNAPII elongation, stalling and/or collapse of the replication fork, and the formation of double-strand DNA breaks that promote cell death.[20–23] Thus, DNA relaxation is achieved through a balancing act of stimulating TOP1 activity while preventing TOP1 from aberrantly remaining bound to ssDNA nicks.[4,6,7] Several mechanisms are known to stimulate TOP1 activity. For example, several transcription factors including wild-type (WT) and mutant p53, MYC,

Please cite this article in press as: Bhola et al., RNA interacts with topoisomerase I to adjust DNA topology, Molecular Cell (2024), https://doi.org/10.1016/j.molcel.2024.07.032

ARF, and NKX3.1 stimulate TOP1 activity.[16,24–27] Also, SV40 virus large T antigen of simian virus 40[28] and the Werner protein, a DNA helicase required for genomic stability[29] stimulate TOP1 activity. TOP1 relaxation activity is also enhanced in gene bodies when TOP1 interacts with bromodomain containing 4 (BRD4)-dependent phosphorylated C-terminal domain of RNAPII.[7] On the flip side of the coin, there are fewer regulators known to attenuate TOP1 activity. Specifically, TOP1 interactions with the tumor suppressor prostate apoptosis response 4 (PAR-4) are known to sequester TOP1 from DNA to prevent TOP1-induced genomic instability.[30] Also, perturbations in DNA structure, such as abasic or apurinic/apyrimidinic (AP) sites, which are intermediates in base excision repair, can hinder TOP1 from accessing sites with certain types of DNA damage.[31] These studies underscore the significance of identifying additional regulators of TOP1 activity that ensure proper dissipation of torsional stress during transcription.

Recent unbiased proteomic studies have identified TOP1 among the growing number of RNA-binding proteins (RBPs) that play key roles in chromatin and gene regulation.[32–34] Also, long non-coding RNA (lncRNA) NORAD was found to interact with RNA binding motif protein X-linked (RBMX) to assemble a ribonucleoprotein complex consisting of TOP1 that maintains genomic stability.[35] TOP1 has also been shown to be among the factors that exhibit RNA dependency in the formation of their protein interactome.[36] While these studies suggest the significance of TOP1 as an RBP, it remains to be elucidated whether TOP1 directly binds RNA, the different types of RNAs that TOP1 binds, and the role of RNA in regulating the classical relaxation of supercoiled DNA by TOP1.

In this study, we mapped TOP1ccs to reveal that TOP1 activity accumulates at active enhancers and protein-coding genes. Moreover, we find that the levels of TOP1cc enrichment at enhancers and protein-coding genes parallel with enhancer and protein-coding transcription levels. TOP1cc enrichment varies across protein-coding genes. Specifically, we find that there exists a focused peak of TOP1cc enrichment upstream of the transcription start site (TSS) and lower-level enrichment of TOP1ccs across gene bodies. TOP1cc accumulation at promoter regions serves as a proxy for preserved negative supercoils that promote transcription initiation through promoter melting and PIC formation.[11,12] Moreover, lower TOP1cc levels present over the bodies of active genes are consistent with lower levels of TOP1 activity needed to relax transcription-coupled torsional stress. We unveil that RNA through TOP1-RNA interactions acts to regulate the lower levels of TOP1 activity across the bodies of protein-coding genes. This RNA-based mechanism has important implications for the proper tuning of TOP1 relaxation of transcription-generated supercoils.

RESULTS

TOP1 enzymatic activity is enriched at active enhancers and gene loci in colon cancer cells

To determine where TOP1 is catalytically active across the colon cancer genome, we used our previously published TOP1cc sequencing (TOP1cc-seq) data in SW480 cells.[37] TOP1cc-seq is a modified chromatin immunoprecipitation sequencing (ChIP-seq) method that maps catalytically engaged complexes.[7] SW480 cells were treated for 4 min with the TOP1-selective inhibitor, camptothecin (CPT) to trap the enzyme in its catalytically engaged form on DNA without altering the chromatin state.[7] Across the colon cancer genome, high levels of TOP1cc enrichment were identified at gene promoters (Figure 1A). These findings demonstrate that the catalytic engagement of TOP1 includes a sharp peak of TOP1cc engaged with DNA upstream of TSSs and lower TOP1cc levels spanning from TSSs to transcription end sites (TESs) (Figure 1A).

Previously, TOP1cc enrichment was observed at enhancers that become activated upon estrogen (E2) treatment.[38] To examine whether TOP1ccs are enriched at active enhancers in SW480 cells, we used our previously published ChIP-seq data for histone marks, histone H3 lysine 27 acetylation (H3K27ac), and histone H3 lysine 4 monomethylation (H3K4me1) that demarcate active enhancers.[39] Given that active enhancers support enhancer RNA (eRNA) synthesis, we also analyzed our published precision run-on sequencing (PRO-seq) data[37] to assay nascent transcription in SW480 cells. Comparative analysis of our H3K4me1 and H3K27ac ChIP-seq and PRO-seq data revealed a substantial number (n = 7,843) of active enhancers in SW480 cells (Figure S1A).

To investigate whether TOP1 catalytic activity is highly concordant with transcriptional output at active enhancers and gene bodies, we parsed TOP1cc accumulation according to transcription levels. Specifically, using our PRO-seq data, we binned protein-coding genes and enhancers according to transcription signal into low (bottom 30%), medium (30%–90%), and high (90%–100%) subsets (Figure S1B). As shown in Figure 1B, peak TOP1cc accumulation was identified at the TSSs of medium and highly transcribed genes (left) and active enhancers binned in the highly transcribed subsets (right). In comparison, low/negligible TOP1cc levels are present at genes (left) and enhancers (right) with low transcription levels (Figure 1B). Relative to genes transcribed at low and medium levels, highly transcribed genes revealed higher level enrichment of TOP1cc accumulation both upstream of the TSSs and across gene bodies (Figure 1B, left). The increased TOP1cc enrichment levels at medium and highly transcribed genes and highly transcribed enhancers are consistent with increased supercoiling that parallels with high transcription levels. Moreover, TOP1cc enrichment at protein-coding genes was further evidenced at the *XPO1* (Figure 1C, top), *PLEKHB2*, and *EXOSC3* genes (Figure S1C, left). TOP1cc enrichment at active enhancers was further evidenced at the *MYC* enhancer (Figure 1C, bottom) and *TRIML2* and *ANKRD55* enhancers (Figure S1C, right). To confirm our TOP1cc-seq data, TOP1cc-qPCR analyses further revealed significant TOP1cc enrichment at the *XPO1* gene promoter and *MYC* enhancer (Figure 1D). The strong parallel in the enrichment of TOP1cc accumulation and transcription levels is consistent with the importance of TOP1 activity at highly active enhancers and gene bodies in colon cancer cells.

The TOP1-associating protein network is composed of RNA regulatory factors

To dissect TOP1 functions at a mechanistic level in colon cancer cells, we performed proteomic analyses to identify functional

Please cite this article in press as: Bhola et al., RNA interacts with topoisomerase I to adjust DNA topology, Molecular Cell (2024), https://doi.org/10.1016/j.molcel.2024.07.032

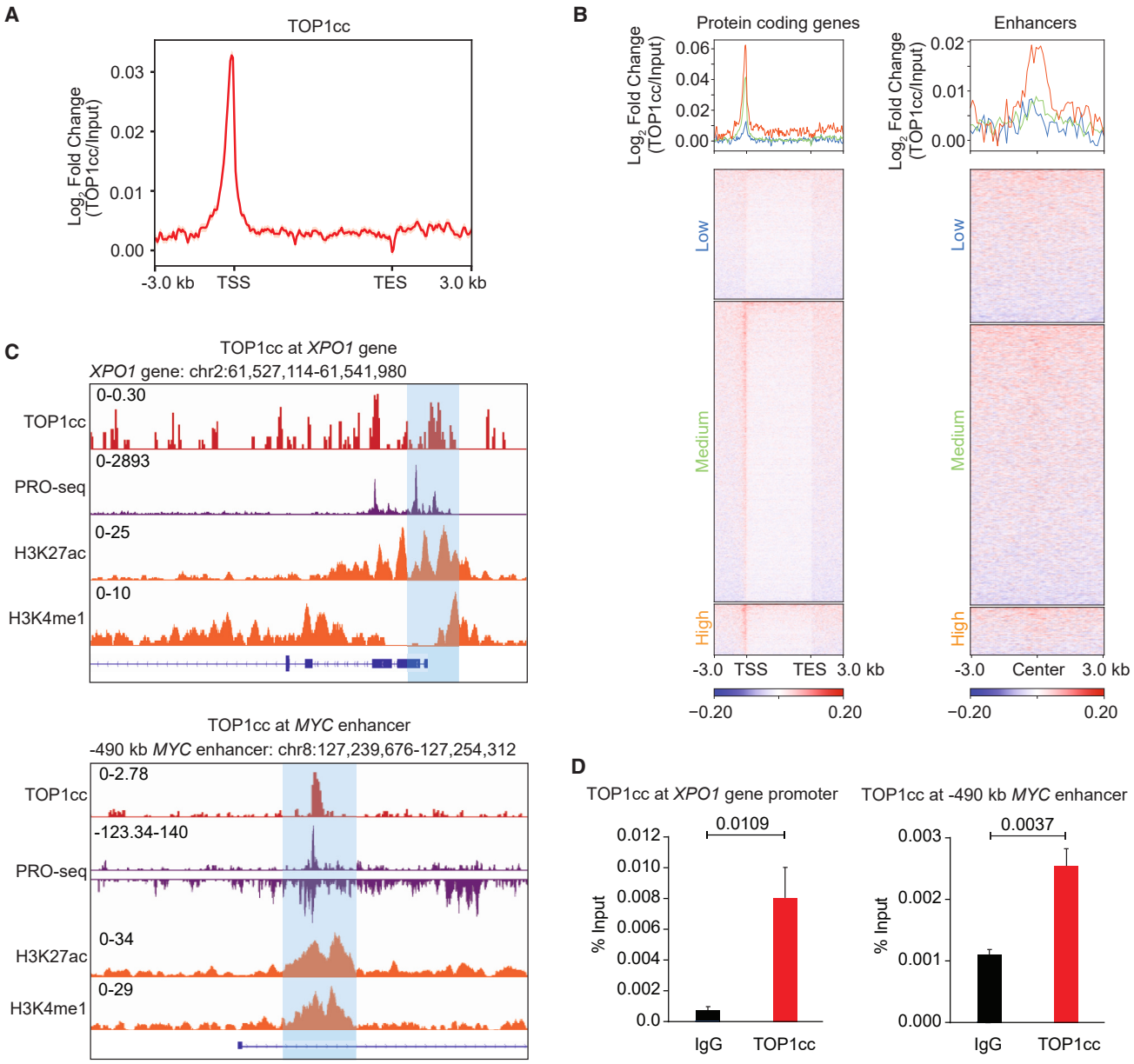

Figure 1. TOP1 enzymatic activity is enriched at active enhancers and gene loci in colon cancer cells

(A) Metaplot of TOP1cc-seq signal across protein-coding genes in SW480 cells. TOP1cc-seq signal is represented as $\log_2$-transformed fold change of bins per million (BPM) over Input and spans 3 kb upstream of the TSS and 3 kb downstream of the TES.

(B) Heatmaps and metaplots of TOP1cc enrichment at (left) protein-coding genes and (right) enhancers (centered on PRO-seq peaks) with low, medium, and high PRO-seq signal in SW480 cells. TOP1cc signal is represented as $\log_2$-transformed fold change of BPM over Input and spans 3 kb upstream of the TSS and 3 kb downstream of the TES and ±3 kb centered on PRO-seq peaks.

(C) Integrative Genomics Viewer (IGV) tracks for TOP1cc, H3K27ac, H3K4me1, and PRO-seq signals at (top) *XPO1* gene locus and (bottom) the *MYC* enhancer in SW480 cells. TOP1cc, H3K27ac, H3K4me1 signal are represented as $\log_2$-transformed fold change of BPM over input. PRO-seq signal is represented as reads per kilobase million (RPKM). The blue shaded region denotes the *XPO1* promoter and *MYC* enhancer. The analyzed coordinates are shown.

(D) TOP1cc-qPCR analyses of IgG and TOP1cc enrichment at (left) *XPO1* gene promoter and (right) *MYC* enhancer in SW480 cells. Data represent the mean and SEM of three independent replicates. Statistical significance was determined by one-tailed Student's t test. p value = 0.0109 at *XPO1* promoter and p value = 0.0037 at *MYC* enhancer.

See also Figure S1 and Table S4.

Please cite this article in press as: Bhola et al., RNA interacts with topoisomerase I to adjust DNA topology, Molecular Cell (2024), https://doi.org/10.1016/j.molcel.2024.07.032

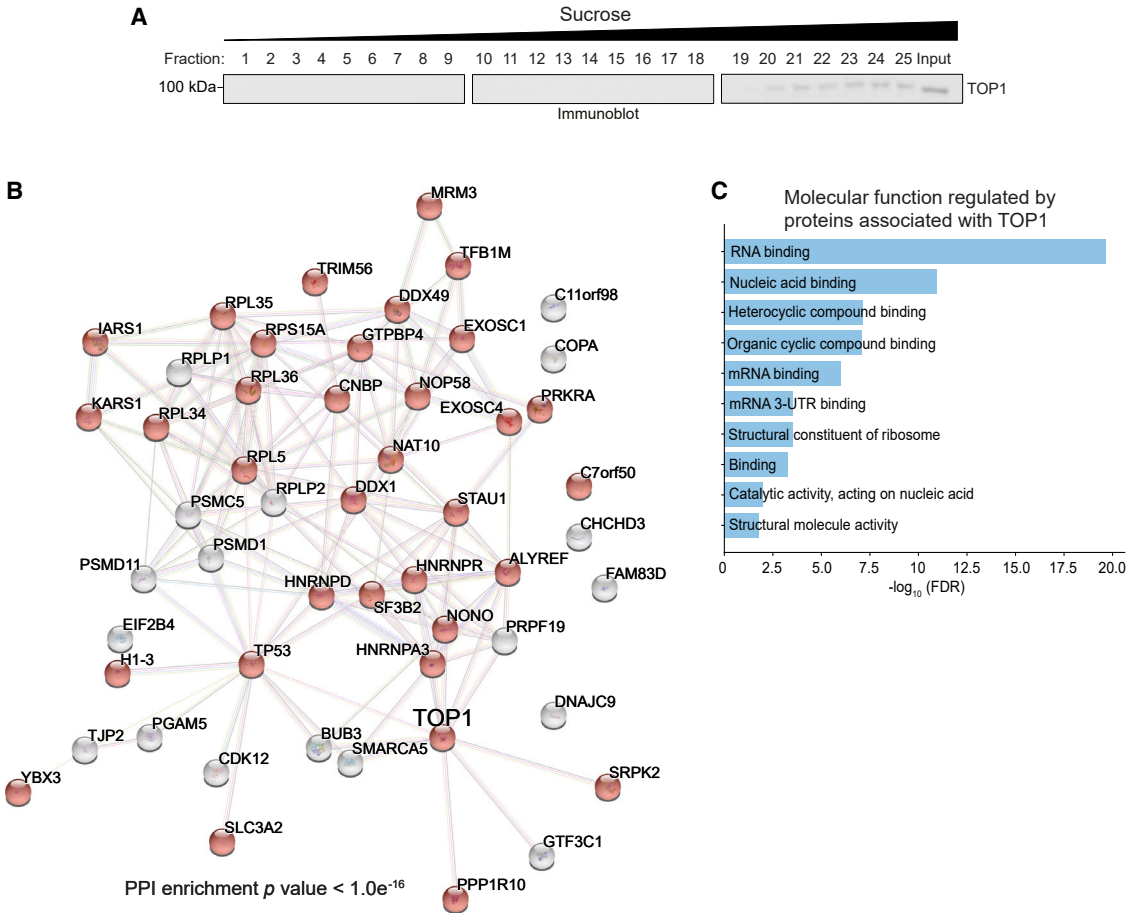

Figure 2. Identification of the TOP1 interactome

(A) Immunoblot analysis of TOP1 from the 25 collected fractions following sucrose-density ultracentrifugation in SW480 cells. A representative image is shown that is representative of three independent experiments.

(B) STRING analysis[42] of 54 proteins identified by TOP1 IP followed by MS in SW480 cells. All proteins are visualized as nodes with the weight of the edges connecting the nodes indicating the confidence of the interactions. The protein-protein interaction (PPI) enrichment is p value < $1.0e^{-16}$. The TOP1-associating proteins present in the most significant GO class that includes RNA binding are shown in red.

(C) Bar graphs depicting the 10 most significantly enriched molecular processes (false discovery rate [FDR] < 0.05) from GO in order of increasing FDR for the proteins identified in Figure 2B.

See also Table S1.

associations of TOP1. Toward this goal, we prepared SW480 whole-cell lysates subjected to sucrose-density gradient ultracentrifugation. As shown in Figure 2A, immunoblot analysis of the collected sucrose fractions revealed a primary TOP1 population with TOP1 migrating in the higher (20–25) sucrose fractions. To delineate the functional interaction networks of TOP1, we coupled the sucrose-density gradient fractionation with immunoprecipitation (IP) followed by quantitative liquid chromatography and tandem mass spectrometry (LC-MS/MS) analysis. Specifically, the TOP1-containing fractions (20–25) were pooled and used for immunoglobulin G (IgG) or TOP1 pull-downs. Three independent biological replicates were processed for LC-MS/MS analysis, and the proteins considered for further analyses met the following criteria: (1) common to two of the three TOP1 IP replicates, (2) have a $-\log_{10} p$ value $\geq$ 20, (3) represented by $\geq$2 peptides, and (4) TOP1-unique or $\geq$3-fold more enriched in the TOP1 relative to the IgG IP. TOP1 was recovered with high coverage (30–32 peptides), and a total of 54 proteins were found to be significantly enriched in the TOP1 pull-down compared with IgG samples (Table S1). Among the TOP1 associating proteins, well-known TOP1 binding partner, TP53[27,40,41] was identified (Figure 2B; Table S1). Notably, Gene Ontology (GO) analysis of the TOP1 associating proteins using the Search Tool for the Retrieval of Interacting Genes/Proteins (STRING) database revealed that the most highly enriched protein category are proteins that bind RNA (Figure 2C). Notably, 63% (n = 34) of the TOP1-associating proteins include RBPs (Table S1). These include members of the RNA exosome nuclease complex (EXOSC1 and EXOSC4), ribosomal proteins (RPL34, RPL35, RPL36, RPS15A, and RPL5), RNA stability controls (YBX3), putative RNA helicases DEAD box proteins (DDX49 and DDX1), and heterogeneous nuclear ribonucleoproteins (HNRNPA3,

Please cite this article in press as: Bhola et al., RNA interacts with topoisomerase I to adjust DNA topology, Molecular Cell (2024), https://doi.org/10.1016/j.molcel.2024.07.032

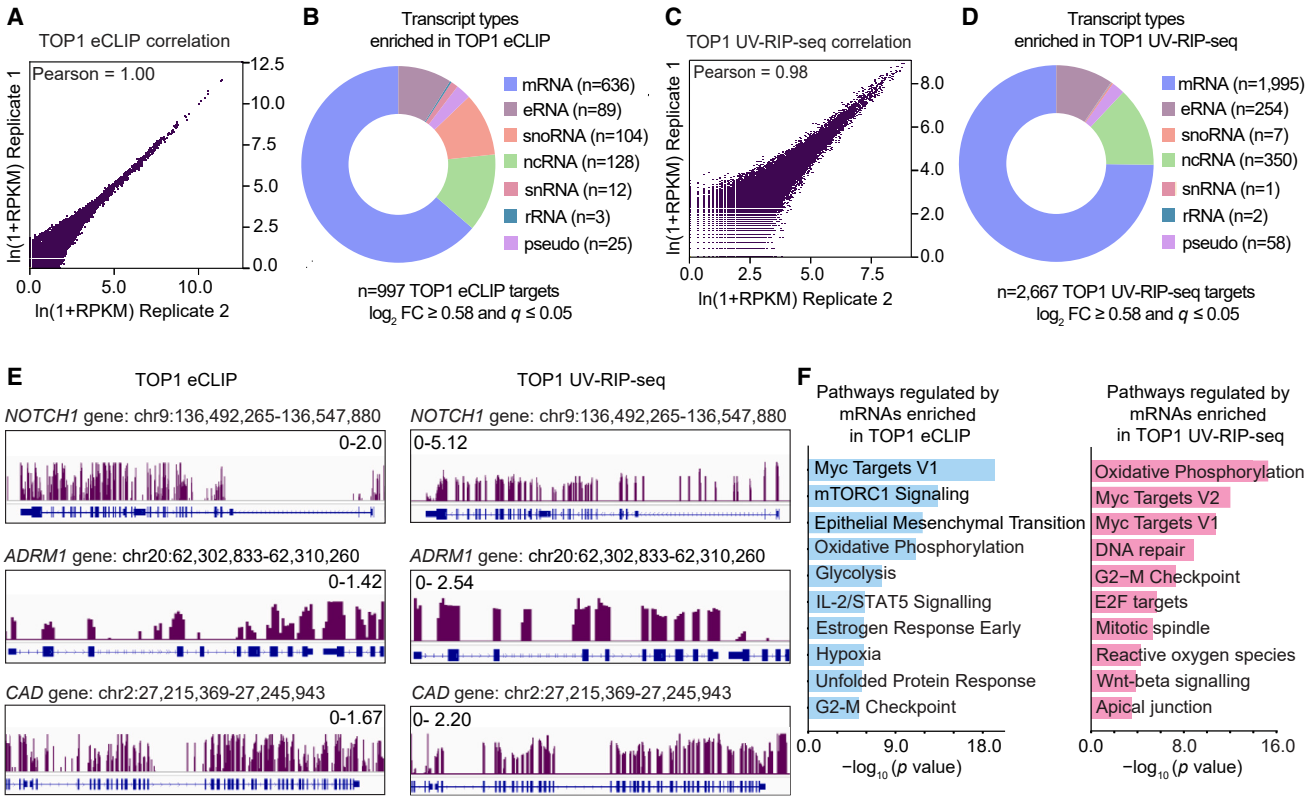

Figure 3. TOP1 is an RBP associated with a broad array of RNAs

(A) Scatterplot of the TOP1 eCLIP read density (as log normalized RPKM) across two biological replicates. Pearson's correlation is 1.00.

(B) Pie chart depicting the different types of RNA species identified by TOP1 eCLIP (n = 997) in two independent replicates. TOP1 eCLIP signal was normalized over IgG eCLIP signal (q value $\leq$ 0.05 and $\log_2$ FC $\geq$ 0.58). eRNAs were identified by overlapping the eCLIP peaks with 7,843 enhancers identified in SW480 cells (Figure S1A).

(C) Scatterplot of the TOP1 UV-RIP-seq read density (as log normalized RPKM) across two biological replicates. Pearson's correlation is 0.98.

(D) Pie chart depicting the number and type of RNA species identified by TOP1 UV-RIP-seq (n = 2,667) in two independent replicates. TOP1 UV-RIP-seq signal was normalized over IgG UV-RIP-seq signal (q value $\leq$ 0.05 and $\log_2$ FC $\geq$ 0.58). eRNAs were identified by overlapping the UV-RIP-seq peaks with 7,843 enhancers identified in SW480 cells (Figure S1A).

(E) IGV tracks for $\log_2$ ratio of TOP1 eCLIP and TOP1 UV-RIP-seq signal (RPKM) over IgG (RPKM) at *NOTCH1*, *ADRM1*, and *CAD* gene loci in SW480 cells. The genome coordinates for each region are shown.

(F) Bar graphs depicting the 10 most significant (p value < 0.05) enriched Molecular Signatures Database (MSigDB) pathways in Enrichr[47] shown in order of decreasing $-\log_{10} p$ value for the TOP1-associating mRNAs identified by eCLIP (left, n = 636 mRNAs) and UV-RIP-seq (right, n = 1,995 mRNAs).

See also Figure S2 and Tables S2 and S3.

HNRNPR, and HNRNPD) (Figure 2B, shown in red). These proteomic analyses revealed a clear association between TOP1 and RBPs, suggesting that TOP1 may also function as an RBP.

TOP1 is an RBP associated with a broad array of RNAs

To identify whether endogenous TOP1 directly binds to cellular RNAs, we performed enhanced cross-linking and IP (eCLIP).[43] Briefly, SW480 cells were subjected to UV cross-linking, treatment with limiting amounts of RNase, and IP using a commercial antibody that specifically enriched for TOP1 (Figure S2A). The RNA fragments protected from RNase digestion by TOP1 protein occupancy were used for generating eCLIP libraries for RNA sequencing (RNA-seq). Scatterplot analysis revealed a positive Pearson correlation coefficient of 1.0 for two TOP1 eCLIP experiments (Figure 3A). In addition, eCLIP libraries were also generated following IP with a nonspecific IgG antibody to discern nonspecific cross-linking events. Relative to the negative control IgG IP, we identified TOP1 enriched ($\log_2$ fold-change (FC) $\geq$ 0.58, q value $\leq$ 0.05) RNAs (n = 997) that include mRNAs (n = 636), eRNAs (n = 89), small nucleolar RNAs (snoRNAs) (n = 104), noncoding RNAs (ncRNAs) (n = 128), small nuclear RNAs (snRNAs) (n = 12), ribosomal RNAs (rRNAs) (n = 3), and pseudo RNAs (n = 25) (Figure 3B; Table S2). As shown in Figure 3B, the majority of TOP1-bound RNAs consist of protein-coding mRNAs (n = 636, 64%). After mRNAs, the next two most abundant classes of RNAs bound by TOP1 include snoRNAs (n = 104, 10%) and ncRNAs (n = 128, 13%). TOP1 binding to mRNAs and snoRNAs is consistent with the efflux of TOP1 between the nucleoplasm and nucleolus, where mRNAs and snoRNAs are widely present, respectively.[44–46] Moreover, analysis of the

Please cite this article in press as: Bhola et al., RNA interacts with topoisomerase I to adjust DNA topology, Molecular Cell (2024), https://doi.org/10.1016/j.molcel.2024.07.032

TOP1 eCLIP signal at protein-coding genes revealed that TOP1 binding to RNA aligns with a sharp peak of TOP1 enrichment at the TSS and broad distribution corresponding to gene bodies before decreasing over the TESs (Figure S2B).

To further our analysis of the transcriptome-wide RNA targets of TOP1 and confirm our eCLIP findings, we performed ultraviolet-cross-linked RNA IP followed by total RNA sequencing (UV-RIP-seq) in SW480 cells. The same antibody against TOP1 used for eCLIP revealed specific enrichment for TOP1 (Figure S2C), and External RNA Controls Consortium (ERCC) spike-in controls were added before the preparation and sequencing of the UV-RIP libraries. Scatterplot analysis revealed a positive Pearson correlation coefficient of 0.98 for the two TOP1 UV-RIP-seq experiments (Figure 3C). Relative to the IgG control, 2,667 high-confidence RNAs ($\log_2$ FC $\geq$ 0.58, q value $\leq$ 0.05) were identified that specifically associate with TOP1 (Figure 3D; Table S3). Consistent with the eCLIP findings (Figure 3B) is the identification that TOP1 associates with similar RNA species, including mRNAs (n = 1,995), eRNAs (n = 254), snoRNAs (n = 7), ncRNAs (n = 350), snRNAs (n = 1), rRNAs (n = 2), and pseudo RNAs (n = 58) (Figure 3D). TOP1-associating eRNAs were identified (Figures 3B and 3D) by overlapping TOP1 UV-RIP-seq and eCLIP peaks with the 7,843 active enhancers identified in Figure S1A. Also similar to the eCLIP analyses, mRNAs (n = 1,995, 75%) were found to be the most prevalent RNA transcripts in association with TOP1 (Figure 3D). We identified 233 mRNAs interacting with TOP1 that are common between the eCLIP and UV-RIP-seq datasets (Figure S2D). The identified association of TOP1 with eRNAs and mRNAs is consistent with TOP1cc enrichment at active enhancers and protein-coding genes (Figure 1B). The overlap between the eCLIP and UV-RIP-seq data is further evidenced by the TOP1 eCLIP (left) and UV-RIP (right) signal that is enriched over exonic regions of *NOTCH1*, *ADRM1*, and *CAD* genes (Figure 3E). Moreover, functional enrichment analysis of TOP1-bound mRNAs identified by eCLIP (Figure 3F, left) and UV-RIP-seq (Figure 3F, right) revealed common pathways that are significantly (p value < 0.05) enriched and associated with cancer progression pathways, including MYC targets, oxidative phosphorylation, and G2-M checkpoint. As shown in Figure S2E, TOP1 UV-RIP followed by qPCR confirmed TOP1 associations with *NOTCH1, TK1, and CAD* mRNAs that are significantly enriched in both the TOP1 eCLIP (Figure 3B; Table S2) and UV-RIP-seq (Figure 3D; Table S3) datasets in SW480 cells. We further validated TOP1 associations with *NOTCH1*, *TK1*, and *CAD* mRNAs in a second colon cancer HCT116 cell line (Figure S2F). The higher number of specific RNA transcripts including mRNAs and eRNAs, identified in the UV-RIP-seq versus eCLIP data (Figure 3D versus 3B), may be due to the more stringent eCLIP approach and based on total RNA-seq versus mRNA-seq approaches used for the sequencing of the UV-RIP and eCLIP libraries, respectively. UV-RIP followed by total RNA-seq would be expected to identify a broader range of RNA interactions, such as low-abundance ncRNAs, including eRNAs. Taken together, our results provide evidence of TOP1 binding to transcripts genome-wide and reveal that TOP1 largely binds to specific mRNAs with known roles in cancer development and progression.

TOP1 directly and comparably binds RNA and DNA

Given that TOP1 forms physiological associations with cellular RNAs, we next examined whether TOP1 directly binds RNA. To this end, we *in vitro* transcribed, folded, and tested several different RNAs for direct interactions with recombinant full-length human TOP1 protein (Figure S3A). We found that TOP1 directly interacts with the different RNA sequences, including 45*S* rRNA, *CCL2* eRNA, *MMP9* eRNA, and *MYC* eRNA (Figure 4A). In comparison, we did not identify TOP1 interactions with Isoleucine transfer RNA (tRNA) from *Mycobacterium tuberculosis* (Figure 4A). To further assess direct TOP1-RNA interactions, we performed electrophoretic mobility shift assays (EMSAs) with ^{32}P-labeled *in vitro*-transcribed and refolded RNA that was incubated with increasing amounts of TOP1 protein. *PNP* mRNA but not *ACSL1* mRNA was identified to significantly associate with endogenous TOP1 in the UV-RIP-seq data in SW480 cells (Figure 3D; Table S3). Consistent with this finding, we identified that TOP1 forms a single prominent complex with *PNP* but showed little to no binding to the *ACSL1* mRNA, which is consistent with direct TOP1 interactions with the *PNP* but not *ACSL1* mRNA (Figure 4B). We also examined whether TOP1 preferentially binds to single-stranded (ssRNA) versus double-stranded (dsRNA) RNA. Notably, while TOP1 directly binds *PNP* ssRNA, TOP1 showed little to no binding to *PNP* dsRNA (Figure 4C). These findings are consistent with TOP1 displaying direct binding to RNA, and taken together with our eCLIP and UV-RIP-seq data, they provide evidence that TOP1 is an RBP.

We next sought to assess how TOP1-RNA associations compare to their well-known DNA interactions. First, EMSAs were performed using equimolar amounts of ^{32}P-labeled *in vitro*-transcribed RNA or a corresponding double-stranded DNA (dsDNA) probe. The DNA and RNA probes correspond with the *MMP9* enhancer region and the *MMP9* eRNA produced by *in vitro* transcription from this enhancer region, respectively. Single prominent complexes were identified that are consistent with direct TOP1 interactions with the *MMP9* dsDNA and *MMP9* eRNA (Figure 4D). Similarly, we extended this finding to a second pair of DNA and RNA probes corresponding to the *CCL2* enhancer region, which revealed that TOP1 directly binds the *CCL2* dsDNA and *CCL2* eRNA (Figure S3B). Comparative analysis of the DNA versus RNA EMSAs at the lower doses of TOP1 protein addition revealed less free RNA versus DNA probe, suggesting that TOP1 more readily binds RNA versus DNA. Quantification of the DNA and RNA EMSAs revealed that TOP1 bound to 31% and 24% of the *MMP9 and CCL2* dsDNAs as compared with 79% and 50% of the *MMP9* and *CCL2* eRNAs at the lowest titration of TOP1 (Figures 4D, right, and S3B, right). This finding is consistent with TOP1 showing strong RNA-binding affinity *in vitro*.

To gain additional biophysical insights into the RNA versus DNA binding kinetics of TOP1, we performed biolayer interferometry (BLI) experiments using the *MYC* eRNA and *PNP* mRNA, which associate with TOP1 in cells (Figure S3C) and *in vitro* (Figures 4A–4C). *MYC* eRNA, *MYC* dsDNA, *PNP* mRNA, or *PNP* dsDNA were biotinylated and immobilized using the streptavidin-biotin capturing method, and the binding affinity of TOP1 was determined by flowing increasing concentrations (0.1, 0.25, 0.5, 0.75, and 1.0 μM) of TOP1. The resulting

Please cite this article in press as: Bhola et al., RNA interacts with topoisomerase I to adjust DNA topology, Molecular Cell (2024), https://doi.org/10.1016/j.molcel.2024.07.032

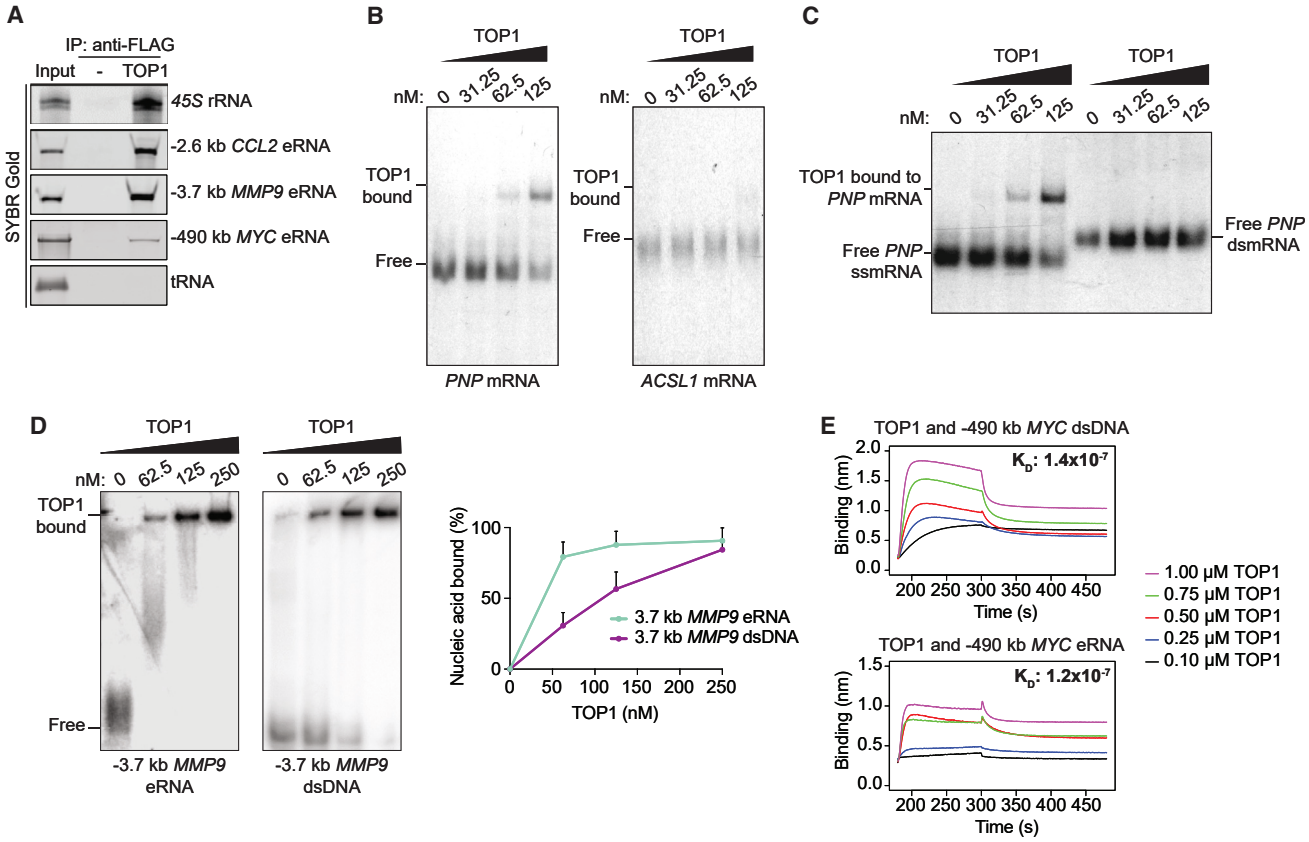

Figure 4. TOP1 directly binds RNA

(A) *In vitro* pull-down of *in vitro*-transcribed *45S* rRNA, *CCL2* eRNA, *MMP9* eRNA, *MYC* eRNA, and tRNA with FLAG-tagged TOP1 protein as revealed by SYBR Gold staining. A representative image of three independent experiments is shown.

(B) EMSA performed with *in vitro* transcribed and refolded ^{32}P-labeled *PNP* mRNA (left) and *ACSL1* mRNA (right) and titrations (0, 31.25, 62.5, and 125 nM) of recombinant TOP1 protein. Probe length: *PNP* mRNA = 230 bp, *ACSL1* mRNA = 130 bp. A representative image of three independent experiments is shown.

(C) EMSA performed with *in vitro* transcribed and refolded ^{32}P-labeled *PNP* ssmRNA and *PNP* dsmRNA and titrations (0, 31.25, 62.5, and 125 nM) of recombinant TOP1 protein. A representative image of three independent experiments is shown.

(D) EMSA performed with *MMP9* dsDNA or *in vitro* transcribed and refolded ^{32}P-labeled *MMP9* eRNA and titrations (0, 62.5, 125, and 250 nM) of recombinant TOP1 protein. Probe length: *MMP9* eRNA = 260 bp, *MMP9* dsDNA = 260 bp. A representative image of three independent experiments is shown. The quantification of the three independent autoradiograms is shown.

(E) Binding analysis of TOP1 to immobilized biotin-labeled (top) *MYC* dsDNA and (bottom) *in vitro* transcribed and refolded *MYC* eRNA as measured in binding response (nm) by BLI. Representative sensorgrams were obtained from injections of 0.10, 0.25, 0.5, 0.75, and 1.0 μM of TOP1. The K_D of three independent experiments is shown.

See also Figure S3 and Table S4.

sensorgrams revealed dose-dependent increases in the binding of TOP1 to the *MYC* dsDNA and *MYC* eRNA (Figure 4E) and to the *PNP* dsDNA and *PNP* mRNA (Figure S3D). Notably, we also measured an apparent equilibrium dissociation constant (K_D) of 1.4 × 10^{-7} and 1.2 × 10^{-7} nM for TOP1 binding to *MYC* dsDNA (top) and *MYC* eRNA (bottom), respectively (Figure 4E) and 3.0 × 10^{-8} and 6.8 × 10^{-8} nM for TOP1 binding to *PNP* dsDNA (left) and *PNP* mRNA (right) (Figure S3C), respectively. These findings are consistent with TOP1 binding to both RNA and DNA with binding constants in the low nanomolar range. Our BLI experiments taken together with our EMSA data reveal that the RNA and DNA pairs examined demonstrate TOP1's ability to directly bind RNA and DNA with a strong and comparable binding affinity *in vitro*.

RNA inhibits TOP1 DNA relaxation in real time

To determine whether RNAs modulate TOP1's ability to relax supercoiled DNA, we performed TOP1 supercoiled DNA relaxation assays.[48] Using purified TOP1 protein (Figure S3A), we measured TOP1's ability to relax negatively supercoiled plasmid DNA. As shown in Figure 5A, lane 2 versus 1, TOP1 efficiently relaxes the supercoiled plasmid DNA as revealed by the nearly complete loss of supercoiled DNA and a significant and corresponding increase in relaxed and nicked DNA species. To measure the roles of RNA in regulating TOP1 enzymatic activity, we examined *in vitro* transcribed and folded *MYC* eRNA in our DNA relaxation assays since this eRNA directly interacts (Figures 4A and 4E) and associates with TOP1 in cells (Figure S3C). As negative controls, we also tested *ACSL1* mRNA

Please cite this article in press as: Bhola et al., RNA interacts with topoisomerase I to adjust DNA topology, Molecular Cell (2024), https://doi.org/10.1016/j.molcel.2024.07.032

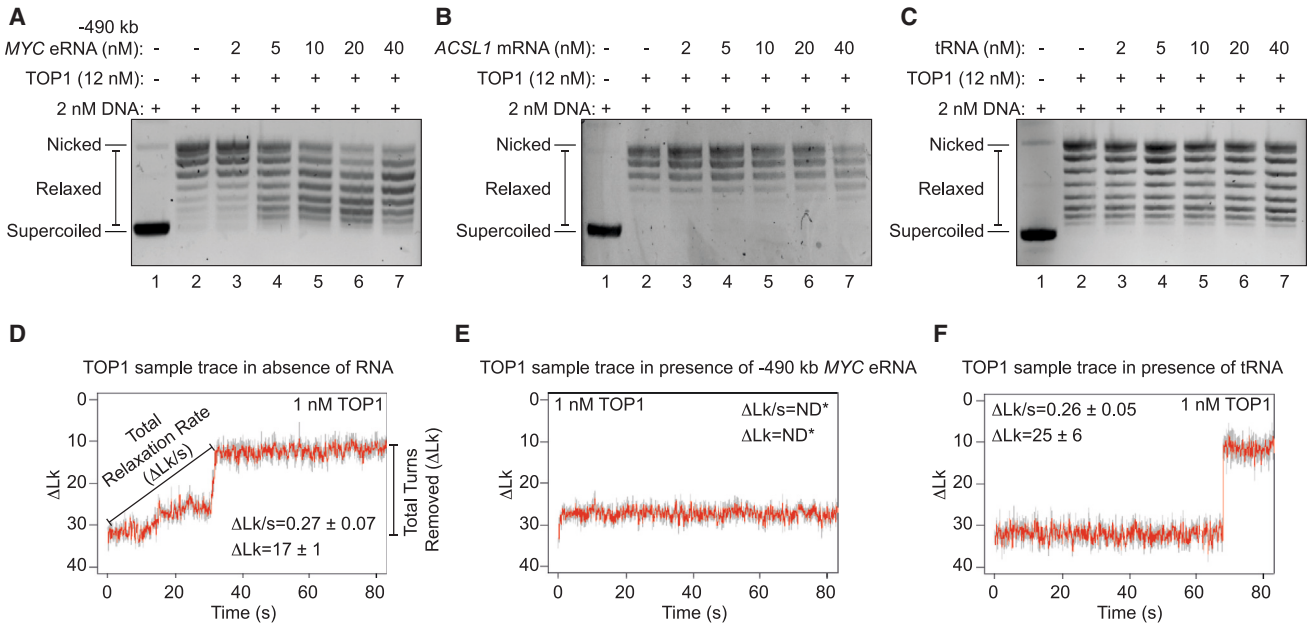

Figure 5. TOP1 catalytic activity is modulated by RNA *in vitro*

(A–C) (A) Plasmid relaxation assay with TOP1 pre-incubated for 5 min in the absence or presence of increasing amounts (2, 5, 10, 20, and 40 nM) of *in vitro* transcribed and refolded *MYC* eRNA, (B) *ACSL1* mRNA, or (C) tRNA, before the addition of 2 nM plasmid DNA. Samples were subjected to 0.8% agarose gel electrophoresis and visualized by staining with ethidium bromide after running the gel. A representative image of three independent experiments is shown.

(D–F) Single-molecule TOP1 relaxation assays in the absence (D) or presence of *MYC* eRNA (E) or tRNA (F). All experiments were performed at 25°C and 0.5 pN force with the measurements denoted in each subpanel and the 10-point moving average is shown in red.

See also Figure S4 and Table S4.

and tRNA, which do not interact with TOP1 (Figures 4A and 4B). eRNA titration experiments revealed that increasing amounts (5–40 nM) of *MYC* eRNA significantly decreased the nicked and relaxed forms of DNA in the presence of TOP1 (Figure 5A, lanes 4–7). In comparison, a lower dose of the *MYC* eRNA (2 nM) showed little to no effect on TOP1's DNA relaxation ability (Figure 5A, lanes 3 versus 2). As expected, increasing amounts of *ACSL1* mRNA and tRNA showed no effect on TOP1 activity as evidenced by the comparable and complete relaxation of DNA in the presence (Figures 5B and 5C lanes 3–7) versus absence of *ACSL1* mRNA and tRNA (Figures 5B and 5C lane 2). These data are consistent with TOP1-binding-specific RNAs that function to potently inhibit TOP1 catalytic activity.

To gain additional insight into RNA inhibition of DNA relaxation rates in real time, we carried out single-molecule DNA supercoil relaxation assays. All single-molecule micromanipulations and measurements were collected using magnetic tweezers as previously described.[49,50] All experiments were performed by introducing a rotation of the magnet to supercoil the DNA while pulling with a force of 0.5 pN.[51] The DNA tether was verified to be a single, intact DNA molecule through a series of calibrations (Figure S4), and the linear portion of the change in linking number (ΔLk) versus extension calibration curve was used to convert DNA extension (μm) to change in linking number. We measured the DNA relaxation rate and change in the number of turns relaxed per second by TOP1 in the absence (Figure 5D) or presence of *MYC* eRNA (Figure 5E) or tRNA (Figure 5F). In the absence of RNA, a burst in TOP1 activity can be observed after ~30 s. and a mean number of 17 ± 1 turn is removed by TOP1 during each relaxation cycle with the total relaxation rate measuring 0.27 ± 0.07 $\Delta Lk \cdot s^{-1}$ (Figure 5D). Notably, the addition of the refolded *MYC* eRNA significantly interfered with TOP1 catalytic activity (Figure 5E). In 9 out of 10 instances, TOP1 relaxation activity could not be measured even after 600 s in the presence of the *MYC* eRNA (Figure 5E). Due to potent RNA inhibition of TOP1 activity, the number of turns removed and relaxation rate were not able to be discerned from the one measurable instance of relaxation. Moreover, for this single instance, we found that DNA could be re-supercoiled readily after relaxation, thereby ruling out religation inhibition by the *MYC* eRNA. Notably, and in contrast to the *MYC* eRNA, we found that tRNA addition resulted in a burst in TOP1 activity that was moderately delayed from ~30 s. in the absence of RNA to ~65 s. in the presence of tRNA (Figure 5F). However, despite this delay, the tRNA exhibited no other discernible effects on TOP1 relaxation activity (Figure 5F), which is consistent with TOP1 interacting with the *MYC* eRNA but not tRNA (Figure 4A). Specifically, we found the total relaxation rate measuring at 0.26 ± 0.05 $\Delta Lk \cdot s^{-1}$ and the number of 25 ± 6 turns removed by TOP1 in the presence of tRNA was comparable to TOP1 in the absence of RNA (Figures 5F versus 5D). Taken together, these data support our supercoiling DNA relaxation assays by revealing that RNA is a potent negative regulator of TOP1 relaxation activity.

Please cite this article in press as: Bhola et al., RNA interacts with topoisomerase I to adjust DNA topology, Molecular Cell (2024), https://doi.org/10.1016/j.molcel.2024.07.032

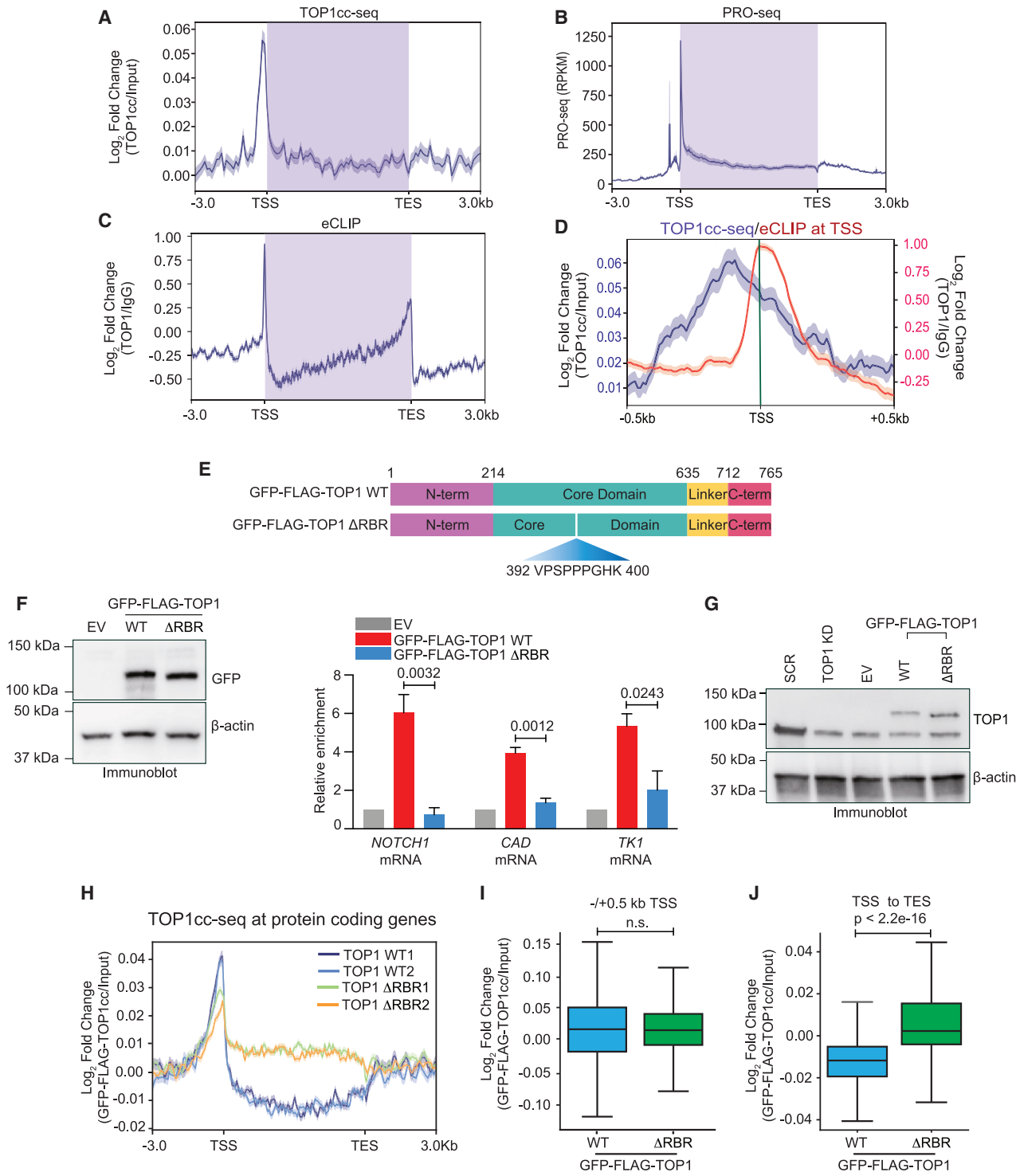

Figure 6. TOP1-RNA interactions inhibit TOP1 DNA relaxation across protein-coding genes

(A) Metaplot of TOP1cc signal at 636 mRNAs that were identified to significantly interact with TOP1 in the TOP1 eCLIP experiment (Figure 3B) in SW480 cells. The TOP1cc-seq signal is represented as $\log_2$-transformed fold change of BPM over Input. The purple area represents the coding region between the TSS and TES.

(B) Metaplot of PRO-seq signal represented as RPKM and spans 3 kb upstream of the TSS and 3 kb downstream of the TES.

(C) Metaplot of eCLIP signal represented as $\log_2$-transformed fold change of RPKM over IgG and spans 3 kb upstream of the TSS and 3 kb downstream of the TES.

(D) A metaplot focused on the TOP1cc and eCLIP signal 0.5 kb upstream and 0.5 kb downstream of the TSS at the 636 mRNAs eCLIP targets.

(legend continued on next page)

Please cite this article in press as: Bhola et al., RNA interacts with topoisomerase I to adjust DNA topology, Molecular Cell (2024), https://doi.org/10.1016/j.molcel.2024.07.032

RNAs bind the TOP1 core domain to inhibit TOP1 DNA relaxation in the bodies of active genes

Having identified that RNA inhibits TOP1 DNA relaxation *in vitro*, we next investigated whether RNA acts to inhibit TOP1 catalytic activity at endogenous gene loci in cells. First, we performed comparative analysis of our TOP1cc-seq, TOP1 eCLIP, and PRO-seq data to systematically identify whether TOP1 interactions with RNA overlap with TOP1cc on DNA. Specifically, metagene analysis identified a strong overlap between TOP1cc accumulation (Figure 6A) and all 636 TOP1-bound mRNAs identified by eCLIP (Figure 6C). Based on our finding that TOP1 catalytic activity shows high congruence with transcriptional output (Figure 1B), we next binned the 636 TOP1-bound mRNAs according to transcription signal into low (bottom 30%), medium (30%–90%), and high (90%–100%) subsets. Of the 636 TOP1-bound mRNAs, 17, 401, and 218 (~3%, 63%, and 34%) are produced from low, medium, and highly transcribed genes, respectively (Figure S5A). This finding, together with the striking overlap of TOP1cc and TOP1 eCLIP signals, is consistent with TOP1-RNA interactions overlapping with the same genes that require medium to high levels of catalytically engaged TOP1cc. Notably, however, TOP1cc peak enrichment (Figure 6A) is offset from the peak enrichment of TOP1 binding to mRNAs (Figure 6C). This is more readily evidenced when examining TOP1cc-seq and TOP1 eCLIP-seq signal −0.5 kb upstream and downstream of the TSS (Figure 6D). Specifically, while TOP1cc peak enrichment is identified upstream of the TSS in the promoter proximal region (−250 bp), TOP1 eCLIP peak enrichment (Figure 6D) overlaps with peak levels of nascent RNA over the TSS as revealed by the PRO-seq signal (Figure 6B). The peak TOP1cc accumulation upstream of the TSS is consistent with TOP1cc regulation of negative DNA supercoiling that facilitates open complex formation by RNAPII.[52] Moreover, the significant decrease in TOP1cc levels that occurs past the TSS and corresponds with increased TOP1-RNA interactions suggested that RNA production may be associated with lower TOP1cc levels during RNAPII-dependent transcription.

To investigate the role that RNA plays in regulating TOP1 activity in cells, we first determined the TOP1 protein domain required for RNA interactions. Toward this goal, we took advantage of the RNA-binding region identification (RBR-ID) tool.[34,53] This RNA-protein UV cross-linking method is believed to reflect direct RNA-protein interactions that are identified by mass spectrometry.[34] Specifically, RBR-ID scores are determined that reflect the combined extent and consistency of depletion (log-converted fold-change between 4-thiouridine (4sU)-treated and non-treated cells) for each residue and serve as a strong metric for protein-RNA cross-linking.[34] The RBR-ID tool revealed the peptide with the maximum RBR-ID score (q value = 0.0024) in the K562 leukemia cell line to overlap with the highly conserved TOP1 DNA binding core domain (TOP1 amino acid [aa] 392–400, VPSPPPGHK) (Figure 6E).[53] To validate the role that this RBR plays in TOP1 binding to RNA, we performed UV-RIP followed by qPCR using SW480 cells transiently transfected with N-terminal GFP-FLAG-tagged TOP1 WT or a GFP-FLAG-tagged TOP1 deletion mutant (TOP1 ΔRBR) that is devoid of the 9 aa (aa 392–400). Both TOP1 WT and TOP1 ΔRBR were comparably expressed (Figure 6F, left). Moreover, co-IP analysis revealed comparable association of TOP1 WT and TOP1 ΔRBR with RNAPII (Figure S5B), which is consistent with the TOP1 ΔRBR mutant forming similar functional associations as its WT counterpart. As shown in Figure 6F (right), UV-RIP-qPCR revealed that relative to the empty vector (EV) control, TOP1 WT robustly immunoprecipitated *NOTCH1* (6-fold), *CAD* (4-fold), *and TK1* (5-fold) mRNAs that are also significantly enriched by endogenous TOP1 in the TOP1 eCLIP (Figure 3B; Table S2), UV-RIP-seq (Figure 3D; Table S3), and UV-RIP-qPCR (Figures S2E and S2F) datasets. Notably, and relative to TOP1 WT, a significant reduction was observed for TOP1 ΔRBR binding to the *NOTCH1* (8-fold), *CAD* (3-fold), and TK1 (3-fold) mRNAs (Figure 6F, right).

To gain insight into the localization and action of TOP1 WT versus TOP1 ΔRBR and examine whether RNA inhibits TOP1 catalytic activity at protein-coding genes, we performed spike-in normalized TOP1cc-seq. Short hairpin RNA (shRNA)-resistant N-terminal tagged GFP-FLAG-TOP1 WT or GFP-FLAG-TOP1 ΔRBR constructs were transiently transfected in SW480 cells stably expressing shRNAs against endogenous TOP1. Relative to the EV control, both TOP1 WT and TOP1 ΔRBR reconstituted TOP1 protein levels to a comparable level in TOP1 knockdown cells (Figure 6G). Following TOP1cc-seq, we parsed the data to systematically identify genes with differential catalytic activity for TOP1 WT versus TOP1 ΔRBR. If RNA negatively modulates

(E) Schematic of TOP1 constructs including TOP1 WT and TOP1 ΔRBR expressed in SW480 cells for UV-RIP-qPCR as shown in (F). TOP1 RNA-binding region was determined by RBR-ID in K562 cell line[53] to be in the TOP1 core domain (392–400 aa, VPSPPPGHK) as denoted.

(F) (Left) Immunoblot analysis of TOP1 and β actin in SW480 cells expressing a pcDNA3.1 (empty vector [EV]) or plasmids expressing N-terminal GFP-FLAG-TOP1 WT or GFP-FLAG-TOP1 ΔRBR. A representative image is shown from at least three independent experiments that were performed. (Right) quantitative reverse-transcription PCR (RT-qPCR) analysis of *NOTCH1*, *CAD*, and *TK1* mRNAs following UV-RIP with GFP antibody and cell lysates prepared from SW480 cells transfected with EV or plasmids expressing N-terminal GFP-FLAG-TOP1 WT or GFP-FLAG-TOP1 ΔRBR. Enrichment levels for each IP are relative to the levels of EV. Data represent the mean and SEM that are representative of at least three independent experiments. Statistical significance was determined by one-tailed Student's t test. *NOTCH1* mRNA p value = 0.0032, *CAD* mRNA p value = 0.0012, and *TK1* mRNA p value = 0.0243.

(G) Immunoblot analysis of TOP1 and β actin in SW480 cells stably expressing TOP1 shRNA and transfected with EV control or shRNA-resistant GFP-FLAG-TOP1 WT or GFP-FLAG-TOP1 ΔRBR. SW480 expressing scramble shRNA (SCR), which does not target genes, was used as a control. A representative image of three independent experiments is shown.

(H) Metaplot analysis of GFP-FLAG-TOP1 WT and GFP-FLAG-TOP1 ΔRBR TOP1cc-seq signal at (n = 3,787) protein-coding genes. GFP-FLAG-TOP1cc-seq signal is represented as $\log_2$-transformed fold change of BPM over Input and spans 3 kb upstream of the TSS and 3 kb downstream of the TES.

(I) Boxplot showing the $\log_2$-transformed fold change (GFP-FLAG-TOP1cc/Input) at promoters (±0.5 kb of TSS) pertaining to the genes analyzed in (H). Statistical significance was determined by Wilcoxon rank-sum test.

(J) Boxplot showing the $\log_2$-transformed fold change (GFP-FLAG-TOP1cc/Input) at coding sequence (CDS) regions pertaining to the genes analyzed in (H). Statistical significance was determined by Wilcoxon rank-sum test.

See also Figure S5 and Table S4.

Please cite this article in press as: Bhola et al., RNA interacts with topoisomerase I to adjust DNA topology, Molecular Cell (2024), https://doi.org/10.1016/j.molcel.2024.07.032

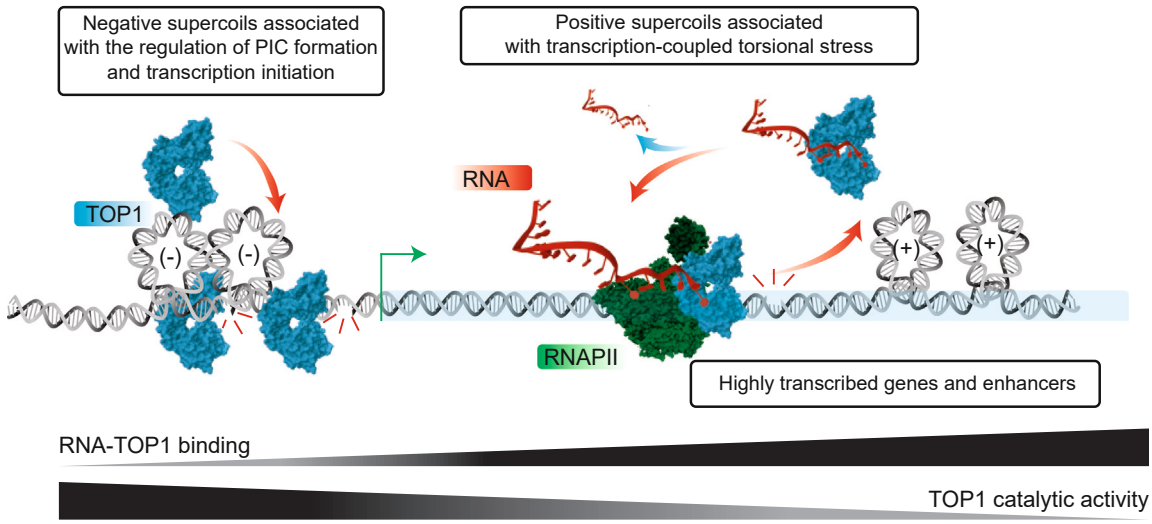

Figure 7. Model for how TOP1-RNA interactions regulate TOP1 activity during RNAPII transcription

We propose a model in which TOP1 activity is enriched in the promoter regions and reduced within the bodies of actively transcribed genes. This dichotomy of TOP1 activity is consistent with TOP1 principally operating to relax negative supercoils associated with the regulation of PIC formation and transcription initiation and, to a lesser extent, to relax transcription-coupled torsional stress. RNA through TOP1-RNA interactions is specifically required for the negative tuning of TOP1 activity over gene bodies. The contributions of RNAPII were not examined in this study, but they were included in the model since RNAPII could also contribute to TOP1 recruitment and activity.[7] See discussion for details. The TOP1 and RNAPII proteins in the model are adapted from PDB: 1A36 and 8H0V.

TOP1ccs, then we expected that the loss of TOP1-RNA interactions would lead to increased levels of TOP1 activity. Consistent with this possibility, metagene profiles for two independent TOP1cc-seq repeats revealed an increase in the input normalized TOP1cc-seq data for TOP1 ΔRBR relative to TOP1 WT across the bodies of a subset (n = 3,787) of genes (Figure 6H). Thus, the importance of TOP1-RNA interactions in regulating TOP1 activity is consistent with the significant increase in activity associated with TOP1 ΔRBR past the TSS and across gene bodies (Figure 6J) and the TOP1-binding profile to RNA (Figure 6C). Based on our finding that TOP1 binding to RNA peaks after the TSS (Figures 6A–6D), we also expected that the activity profiles for TOP1 ΔRBR versus TOP1 WT would be comparable upstream of the TSS in the promoter region. As expected and similar to endogenous TOP1cc enrichment (Figure 6A), peak enrichment of TOP1 WT and TOP1 ΔRBR catalytic engagement is found upstream of the TSSs. Moreover, the promoter proximal enrichment of the TOP1 ΔRBR was comparable to TOP1 WT (Figures 6H and 6I). The slight and non-significant decrease in TOP1 ΔRBR versus TOP1 WT catalytic activity observed at the promoter may relate to the significantly higher levels of activity associated with TOP1 ΔRBR over the respective gene bodies (Figures 6H–6J). Thus, the characteristic profile of TOP1 regulation of negative supercoiling on chromatin that is comparable for the TOP1ΔRBR mutant and TOP1 WT at gene promoters (Figure 6H) and their comparable association with RNAPII (Figure S5) is consistent with TOP1 ΔRBR maintaining its functions on chromatin. Cross-comparative analysis of this subset of genes (n = 3,787) showing increased TOP1 ΔRBR activity and mRNAs significantly ($\log_2$ FC $\geq$ 0.58 and q $\leq$ 0.05) bound by TOP1 revealed a partial overlap. Specifically, we identified 13% (n = 180 of the 636) and ~10% (n = 196 of 1,995) of mRNAs identified by TOP1 eCLIP (Figure 3B) and UV-RIP-seq (Figure 3D), respectively that overlap with the 3,787 genes. This partial overlap was determined by using the stringent cut-off ($\log_2$ FC $\geq$ 0.58 and q $\leq$ 0.05) for establishing significance for TOP1-bound mRNAs but does not exclude that other less significant and enriched TOP1-bound mRNAs may also overlap. Moreover, we cannot exclude the possibility that the TOP1 RNA-binding capability and consequences of TOP1-RNA interactions at specific genes will be differentially regulated by other cellular contributions, including post-translational modifications (PTMs), altered TOP1 and/or RNA conformations, and TOP1 cellular localization. Taken together, these biophysical, biochemical, and cellular findings strongly support a role for RNA in creating a negative feedback loop that lowers the levels of TOP1 catalytic activity, which has important implications for the relaxation of transcription-coupled supercoiling tension (Figure 7).

DISCUSSION

The delicate balance of regulating DNA supercoiling during transcription requires the proper tuning of topoisomerase activity. In prokaryotes, the release of positive and negative supercoiling is facilitated by DNA gyrase and TOPIA, respectively.[54] These separated actions of gyrase and TOPIA are directed by differential substrate preferences with gyrase acting on relaxed versus supercoiled DNA and TOPIA favoring highly negatively supercoiled DNA.[54] Our data support a eukaryotic model for the separation of TOP1 activity across actively transcribed genes that are under the direct control of RNA. We find that TOP1 activity is highly enriched upstream of the TSS in promoter proximal regions and less enriched within actively transcribed gene bodies. This switch in TOP1cc accumulation over actively transcribed

Please cite this article in press as: Bhola et al., RNA interacts with topoisomerase I to adjust DNA topology, Molecular Cell (2024), https://doi.org/10.1016/j.molcel.2024.07.032

genes is consistent with favoring high transcriptional output. Specifically, the high levels of TOP1ccs associated with high torsional stress at promoter regions would favor transcription initiation/reinitiation.[11,12] In comparison, the lower levels of transcription-coupled torsional stress over gene bodies are consistent with TOP1cc draining the positive supercoils that otherwise block RNAPII elongation,[55] while also avoiding overwound DNA that can aberrantly retain TOP1cc and impede RNAPII binding.[56] Our data suggest that by putting TOP1 activity under the direct control of RNA production may effectively manage the distinct supercoiling requirements that are critical for TOP1's contributions to PIC formation/transcription initiation and transcriptional elongation.[55] Coupling TOP1 DNA relaxation to RNA production may impact gene regulation by (1) trapping negative supercoils in gene promoters to facilitate PIC formation and transcription initiation/reinitation,[11,12] (2) preventing premature release of RNAPII into elongation by retaining RNAPII in its paused state, and (3) modulating the levels of positive supercoils that promote the proper control over the rate of RNAPII elongation across genes.[9,10]

This study provides detailed mechanistic insights into TOP1 regulation of transcription-generated supercoils by providing evidence that RNA through TOP1 interactions, significantly decreases TOP1 activity across gene bodies (Figure 7). Our study provides several independent findings to support this identified RNA-based mechanism. First, we unveil that TOP1 is an RBP by demonstrating that TOP1 directly binds a variety of RNA species that predominantly include mRNAs. We also reveal that TOP1 directly and comparably binds to RNA and DNA *in vitro* with a strong binding affinity. Supporting a direct role for TOP1-RNA interactions in preventing TOP1 catalytic activity during transcription is our finding that relative to TOP1 WT, an RNA-binding mutant, TOP1 ΔRBR exhibits comparable activity upstream of the TSS but significantly higher activity across the bodies of protein-coding genes. Notably, specific TOP1-bound RNAs also potently inhibited TOP1 relaxation of DNA *in vitro* in both DNA supercoiling assays and during single-molecule tracking of TOP1 activity in real time.

The growing paradigm that foundational mechanisms underlying transcriptional control involve RBPs[57] is further supported by our interesting finding that TOP1 is an RBP. The defined RNA-based mechanism is consistent with a negative feedback loop for TOP1 relaxation potential specifically during RNAPII transcription of highly active genes. Moreover, the coupling of TOP1 activity to RNA during transcription might also explain a mechanism for countering stimulation of TOP1 activity that is achieved by the transcription machinery during RNAPII elongation.[7] This is considering the previous finding that BRD4 phosphorylates RNAPII to enhance TOP1cc activity to clear RNAPII pausing and transition to productive elongation.[7] A role for RNA through RBPs in preventing premature release into elongation has been suggested for other RBPs including RBFox2 that bind nascent RNA and chromatin near the TSS.[58] By mapping the direct binding landscape of TOP1 along its target RNAs at single nucleotide resolution, we demonstrate that peak-level enrichment of TOP1 binding to mRNAs parallels the actively engaged RNAPII profile as evidenced by our PRO-seq data. The high level of PRO-seq signal over the TSS coupled with lower levels over the gene body is characteristic of promoter proximal pausing of RNAPII before it transitions into productive elongation.[59,60] Moreover, the higher levels of TOP1cc accumulation over gene bodies that we observed for the TOP1 ΔRBR relative to TOP1 WT are a proxy for increased accumulation of positive supercoiling tension that could reflect premature release of paused RNAPII and/or faster elongation rates achieved as RNAPII transitions into elongation. Thus, an intriguing possibility is that TOP1-RNA interactions underlie a common mechanism to control RNAPII pause-release and that loss of these interactions could lead to aberrant release of RNAPII into elongation. Future studies are needed to dissect these possibilities and elucidate the precise functions of RNA molecules in regulating TOP1 activity at enhancers and protein-coding genes and in regulating the RNAPII transcription cycle.

This emerging RNA-centric view of TOP1 as an RBP will undeniably continue to advance our understanding of this essential enzyme. While our study provides evidence to support the role of RNA as a negative modulator of TOP1 catalytic activity, the direct binding of TOP1 to mRNAs across exons could also have important implications for RNA metabolism. Consistent with this possibility is our finding that RBPs are the most significantly enriched and high-confidence binding partners of TOP1. The RBPs associating with TOP1 are well known for influencing multiple aspects of RNA metabolism, including the regulation of RNA stability, translation, degradation, and export. Thus, it will be important to discern whether TOP1 plays critical roles in ensuring the proper processing and function of mRNAs in addition to controlling their expression levels. Moreover, our finding that TOP1 directly binds to mRNA and snoRNAs is consistent with TOP1's well-known role to efflux between the nucleoplasm and nucleolus, respectively.[44–46,61,62] The regulation of TOP1 cellular mobility is only partially understood; thus, it would be interesting to examine whether the nuclear redistribution of TOP1 is impacted by TOP1 binding to snoRNAs and mRNAs. Consistent is the growing support for RNA as a general regulator and important structural component necessary for nucleating the assembly of RBPs into subcompartments including nucleoli.[63] Thus, our finding that TOP1 is an RBP begs many interesting questions that if addressed could provide valuable insights into the multifaceted roles of TOP1.

Our observations that TOP1 binds to specific mRNAs produced from highly active genes and enhancers that are enriched for TOP1cc are consistent with TOP1 binding to endogenous RNAs in a gene and enhancer-specific manner. This finding is consistent with recent studies showing that RBPs, polycomb repressive complex 2 (PRC2),[64–66] CREB binding protein (CBP),[67] and BRD4[68] associate with RNAs produced from the genomic regions that are also occupied by these factors. Moreover, our biochemical findings also revealed that TOP1's relationship with RNA includes a preference for ssRNA versus dsRNA. The negligible levels of TOP1 binding to dsRNA suggest that viral dsRNAs are unlikely to compete for TOP1 interactions during a dsRNA-mediated antiviral response. Thus, this finding is likely to have important implications for ensuring that TOP1-ssRNA interactions are likely to remain coupled to

regulating TOP1's essential role in dissipating supercoiling tension during RNAPII-dependent transcription. Our findings did not rule out potential contributions made by secondary RNA structure or RNA modifications that may also impact TOP1-RNA interactions. Thus, future studies should explore regulatory mechanisms underlying TOP1 binding to RNA. Moreover, while our study sheds light on a variety of RNA species, predominantly mRNAs that are bound by TOP1, we cannot exclude the possibility that the RNA-binding capability and consequences of TOP1-RNA interactions will be differentially regulated and influenced by PTMs, altered TOP1 and/or RNA conformations, and cellular localization.

Consistent with the biological importance of specific TOP1-RNA interactions in colon cancer is the finding that TOP1 predominantly binds mRNAs involved in tumor-promoting pathways. Moreover, based on our findings that these tumor-promoting RNAs inhibit TOP1 cleavage complexes across gene bodies, it suggests that RNA could make TOP1ccs more resistant to anticancer drugs. TOP1ccs are transient and self-reversible with TOP1 switching the DNA back and forth between a nicked and preferred religated state. Stabilizing DNA-TOP1 cleavage complexes to prevent DNA religation ultimately results in cell death and underlies the effectiveness of the TOP1 inhibitor and first-line chemotherapeutic CPT in treating cancer patients.[69] Thus, circumventing RNA inhibition of TOP1ccs at actively transcribed tumor-promoting genes may serve as a druggable node in CRC. Our identification of this TOP1-RNA-dependent regulatory mechanism provides a unique opportunity for future studies to explore the biological significance of TOP1 interactions with cancer-associated transcripts in cancer cells and for testing the development of cutting-edge cancer therapeutics targeting the RNA interface of TOP1.

Limitations of the study

Our study shows evidence that RNA is directly bound by the classical DNA regulator TOP1 and that RNA inhibits TOP1's regulation of transcription-generated positive supercoiling tension. However, our study has not examined the role of RNA in regulating other well-known roles of TOP1 outside of gene regulation including DNA replication, recombination, and chromatin remodeling that may also be influenced by RNA-TOP1 interactions. Moreover, while our study sheds light on a variety of RNA species, predominantly mRNAs that are bound by TOP1, we cannot exclude the possibility that the RNA-binding capability and consequences of TOP1-RNA interactions will be differentially regulated and influenced by PTMs, altered TOP1 and/or RNA conformations, and cellular localization. Moreover, our studies support previous findings[53] that RNA associates with the TOP1 RBR composed of 9 aa within the TOP1 core domain that clamps down on DNA.[70] While our study confirms that this RBR is required for TOP1 RNA interactions, we find that deletion of the RBR does not disrupt TOP1 catalytic activity at gene promoters where it is found to exhibit comparable levels of DNA relaxation as TOP1 WT. Thus, these findings are consistent with the loss of the TOP1 RBR disrupting RNA interactions while maintaining its functions on DNA as demonstrated by its regulation of negative DNA supercoiling. Yet, further work is needed to dissect the breadth of molecular mechanisms underlying the formation of TOP1-RNA interactions and their relationship with chromatin and downstream consequences on TOP1 biology and RNA regulation and function.

STAR★METHODS

Detailed methods are provided in the online version of this paper and include the following:

- KEY RESOURCES TABLE
- RESOURCE AVAILABILITY
  - Lead contact
  - Materials availability
  - Data and code availability
- EXPERIMENTAL MODEL AND STUDY PARTICIPANT DETAILS
  - Cell Culture and Treatments
  - Lentivirus Production and Transduction
- METHOD DETAILS
  - Antibodies
  - Immunoblotting
  - RNA Purification and RT-qPCR
  - Sucrose Density Gradient Ultracentrifugation
  - TOP1 IP Followed by Mass Spectrometry
  - Mass Spectrometry
  - Enhanced Crosslinking IP (eCLIP)
  - Ultraviolet-RNA Immunoprecipitation (UV-RIP)
  - Purification of Recombinant TOP1 Full Length Protein
  - In Vitro RNA synthesis
  - RNA Refolding
  - Electrophoretic Mobility Shift Assays
  - In Vitro Pull-Down RNA binding assays
  - Biolayer-Interferometry (BLI) Assays
  - Co-Immunoprecipitation Assays
  - TOP1cc-Sequencing
  - DNA Supercoiling Assay
  - Single-Molecule Magnetic Tweezer Analysis of TOP1
- QUANTIFICATION AND STATISTICAL ANALYSIS
  - MS Quantitative Analyses
  - ChIP-seq and TOP1cc-seq Analysis
  - eCLIP Analysis
  - UV-RIP-seq and PRO-seq Analysis

SUPPLEMENTAL INFORMATION

Supplemental information can be found online at https://doi.org/10.1016/j.molcel.2024.07.032.

ACKNOWLEDGMENTS

The authors would like to thank Anita Wang for assistance with reagent preparations and experiment coordination and Steve Lauberth for graphic design and figure layout preparation. All mass spectrometry was performed by the Biomolecular and Proteomics Mass Spectrometry Facility, UC San Diego (Majid Ghassemian, PhD, Director). All BLI experiments were performed with the help of the Northwestern University Keck Biophysics Facility. Support from the R.H. Lurie Comprehensive Cancer Center of Northwestern University to the Keck Biophysics Facilities is acknowledged. Research in the Lauberth lab is supported by a grant from the NIH/National Institute of General Medical Sciences (R35 GM128900) to S.M.L. Cancer Center research in the Mondragón Lab is supported by the NIH (R35-GM118108) to A.M. and an NIH NRSA (5T32-GM008382) training grant fellowship to E.T. Research in the John Marko Lab is supported by the NIH (R01-GM105847) to J.F.M. E.L.V.N. is a CPRIT Scholar in Cancer Research (RR200040), and research in the Chuan lab is supported by the following funding: C.H. RM1

HG008935. This material is based upon work supported by the National Science Foundation Graduate Research Fellowship Program (ET) under Grant No. (DGE-2234667). Any opinions, findings, and conclusions or recommendations expressed in this material are those of the author(s) and do not necessarily reflect the views of the National Science Foundation. The research reported in this publication was supported by NIGMS of the National Institutes of Health under award number T32GM140995 (E.T.).

AUTHOR CONTRIBUTIONS

Conceptualization, S.M.L., P.O., H.R., M.B., and K.A.; methodology, most of the experiments were performed by P.O., H.R., K.A., and S.M.L.; computational analysis, H.R., P.O., M.B., K.A., S.M.L., and B.L.; software, M.B.; investigation, P.O., H.R., M.B., K.A., E.T., N.M., B.L., P.A.-L., P.P., J.F.M., S.M.L., and A.C.S.; resources, J.F.M., S.M.L., E.L.V.N., and A.M.; writing – review and editing, S.M.L., E.T., P.O., H.R., A.M., C.H., M.B., K.A., and E.L.V.N.; funding acquisition, S.M.L. All authors critically reviewed the manuscript and approved the final version.

DECLARATION OF INTERESTS

E.L.V.N. is co-founder, member of the Board of Directors, on the SAB, equity holder, and paid consultant for Eclipse BioInnovations. E.L.V.N.'s interests have been reviewed and approved by the Baylor College of Medicine in accordance with its conflict-of-interest policies. C.H. is a scientific founder, a member of the scientific advisory board and equity holder of Aferna Bio, Inc. and Ellis Bio Inc., a scientific co-founder and equity holder of Accent Therapeutics, Inc., and a member of the scientific advisory board of Rona Therapeutics and Element Biosciences.

Received: September 28, 2022
Revised: July 7, 2023
Accepted: July 31, 2024
Published: August 21, 2024

REFERENCES

1. Merino, A., Madden, K.R., Lane, W.S., Champoux, J.J., and Reinberg, D. (1993). DNA topoisomerase I is involved in both repression and activation of transcription. Nature *365*, 227–232. https://doi.org/10.1038/365227a0.
2. Shykind, B.M., Kim, J., Stewart, L., Champoux, J.J., and Sharp, P.A. (1997). Topoisomerase I enhances TFIID-TFIIA complex assembly during activation of transcription. Genes Dev. *11*, 397–407. https://doi.org/10.1101/gad.11.3.397.
3. Durand-Dubief, M., Persson, J., Norman, U., Hartsuiker, E., and Ekwall, K. (2010). Topoisomerase I regulates open chromatin and controls gene expression in vivo. EMBO J. *29*, 2126–2134. https://doi.org/10.1038/emboj.2010.109.
4. Kouzine, F., Gupta, A., Baranello, L., Wojtowicz, D., Ben-Aissa, K., Liu, J., Przytycka, T.M., and Levens, D. (2013). Transcription-dependent dynamic supercoiling is a short-range genomic force. Nat. Struct. Mol. Biol. *20*, 396–403. https://doi.org/10.1038/nsmb.2517.
5. Pedersen, J.M., Fredsoe, J., Roedgaard, M., Andreasen, L., Mundbjerg, K., Kruhøffer, M., Brinch, M., Schierup, M.H., Bjergbaek, L., and Andersen, A.H. (2012). DNA Topoisomerases maintain promoters in a state competent for transcriptional activation in Saccharomyces cerevisiae. PLoS Genet. *8*, e1003128. https://doi.org/10.1371/journal.pgen.1003128.
6. Teves, S.S., and Henikoff, S. (2014). DNA torsion as a feedback mediator of transcription and chromatin dynamics. Nucleus *5*, 211–218. https://doi.org/10.4161/nucl.29086.
7. Baranello, L., Wojtowicz, D., Cui, K., Devaiah, B.N., Chung, H.J., Chan-Salis, K.Y., Guha, R., Wilson, K., Zhang, X., Zhang, H., et al. (2016). RNA Polymerase II Regulates Topoisomerase 1 Activity to Favor Efficient Transcription. Cell *165*, 357–371. https://doi.org/10.1016/j.cell.2016.02.036.
8. Liu, L.F., and Wang, J.C. (1987). Supercoiling of the DNA template during transcription. Proc. Natl. Acad. Sci. USA *84*, 7024–7027. https://doi.org/10.1073/pnas.84.20.7024.
9. Gartenberg, M.R., and Wang, J.C. (1992). Positive supercoiling of DNA greatly diminishes mRNA synthesis in yeast. Proc. Natl. Acad. Sci. USA *89*, 11461–11465. https://doi.org/10.1073/pnas.89.23.11461.
10. Joshi, R.S., Piña, B., and Roca, J. (2010). Positional dependence of transcriptional inhibition by DNA torsional stress in yeast chromosomes. EMBO J. *29*, 740–748. https://doi.org/10.1038/emboj.2009.391.
11. Dunaway, M., and Ostrander, E.A. (1993). Local domains of supercoiling activate a eukaryotic promoter in vivo. Nature *361*, 746–748. https://doi.org/10.1038/361746a0.
12. Parvin, J.D., and Sharp, P.A. (1993). DNA topology and a minimal set of basal factors for transcription by RNA polymerase II. Cell *73*, 533–540. https://doi.org/10.1016/0092-8674(93)90140-l.
13. Rømer, M.U., Jensen, N.F., Nielsen, S.L., Müller, S., Nielsen, K.V., Nielsen, H.J., and Brünner, N. (2012). TOP1 gene copy numbers in colorectal cancer samples and cell lines and their association to in vitro drug sensitivity. Scand. J. Gastroenterol. *47*, 68–79. https://doi.org/10.3109/00365521.2011.638393.
14. Smith, D.H., Christensen, I.J., Jensen, N.F., Markussen, B., Rømer, M.U., Nygård, S.B., Müller, S., Nielsen, H.J., Brünner, N., and Nielsen, K.V. (2013). Mechanisms of topoisomerase I (TOP1) gene copy number increase in a stage III colorectal cancer patient cohort. PLoS One *8*, e60613. https://doi.org/10.1371/journal.pone.0060613.
15. Ogino, M., Fujii, T., Nakazawa, Y., Higuchi, T., Koibuchi, Y., Oyama, T., Horiguchi, J., and Shirabe, K. (2020). Implications of Topoisomerase (TOP1 and TOP2α) Expression in Patients With Breast Cancer. In Vivo *34*, 3483–3487. https://doi.org/10.21873/invivo.12188.
16. Mao, Y., Okada, S., Chang, L.S., and Muller, M.T. (2000). p53 dependence of topoisomerase I recruitment in vivo. Cancer Res. *60*, 4538–4543.
17. Das, S.K., Kuzin, V., Cameron, D.P., Sanford, S., Jha, R.K., Nie, Z., Rosello, M.T., Holewinski, R., Andresson, T., Wisniewski, J., et al. (2022). MYC assembles and stimulates topoisomerases 1 and 2 in a "topoisome". Mol. Cell *82*, 140–158.e12. https://doi.org/10.1016/j.molcel.2021.11.016.
18. Pommier, Y., Sun, Y., Huang, S.N., and Nitiss, J.L. (2016). Roles of eukaryotic topoisomerases in transcription, replication and genomic stability. Nat. Rev. Mol. Cell Biol. *17*, 703–721. https://doi.org/10.1038/nrm.2016.111.
19. Wang, H., Di Gate, R.J., and Seeman, N.C. (1996). An RNA topoisomerase. Proc. Natl. Acad. Sci. USA *93*, 9477–9482. https://doi.org/10.1073/pnas.93.18.9477.
20. Ray Chaudhuri, A., Hashimoto, Y., Herrador, R., Neelsen, K.J., Fachinetti, D., Bermejo, R., Cocito, A., Costanzo, V., and Lopes, M. (2012). Topoisomerase I poisoning results in PARP-mediated replication fork reversal. Nat. Struct. Mol. Biol. *19*, 417–423. https://doi.org/10.1038/nsmb.2258.
21. Koster, D.A., Palle, K., Bot, E.S., Bjornsti, M.A., and Dekker, N.H. (2007). Antitumour drugs impede DNA uncoiling by topoisomerase I. Nature *448*, 213–217. https://doi.org/10.1038/nature05938.
22. Kuzminov, A. (2001). Single-strand interruptions in replicating chromosomes cause double-strand breaks. Proc. Natl. Acad. Sci. USA *98*, 8241–8246. https://doi.org/10.1073/pnas.131009198.
23. Wimberly, H., Shee, C., Thornton, P.C., Sivaramakrishnan, P., Rosenberg, S.M., and Hastings, P.J. (2013). R-loops and nicks initiate DNA breakage and genome instability in non-growing Escherichia coli. Nat. Commun. *4*, 2115. https://doi.org/10.1038/ncomms3115.
24. Bowen, C., Stuart, A., Ju, J.H., Tuan, J., Blonder, J., Conrads, T.P., Veenstra, T.D., and Gelmann, E.P. (2007). NKX3.1 homeodomain protein binds to topoisomerase I and enhances its activity. Cancer Res. *67*, 455–464. https://doi.org/10.1158/0008-5472.CAN-06-1591.

25. Puc, J., Kozbial, P., Li, W., Tan, Y., Liu, Z., Suter, T., Ohgi, K.A., Zhang, J., Aggarwal, A.K., and Rosenfeld, M.G. (2015). Ligand-dependent enhancer activation regulated by topoisomerase-I activity. Cell *160*, 367–380. https://doi.org/10.1016/j.cell.2014.12.023.

26. Karayan, L., Riou, J.F., Séité, P., Migeon, J., Cantereau, A., and Larsen, C.J. (2001). Human ARF protein interacts with topoisomerase I and stimulates its activity. Oncogene *20*, 836–848. https://doi.org/10.1038/sj.onc.1204170.

27. Gobert, C., Skladanowski, A., and Larsen, A.K. (1999). The interaction between p53 and DNA topoisomerase I is regulated differently in cells with wild-type and mutant p53. Proc. Natl. Acad. Sci. USA *96*, 10355–10360. https://doi.org/10.1073/pnas.96.18.10355.

28. Simmons, D.T., Roy, R., Chen, L., Gai, D., and Trowbridge, P.W. (1998). The activity of topoisomerase I is modulated by large T antigen during unwinding of the SV40 origin. J. Biol. Chem. *273*, 20390–20396. https://doi.org/10.1074/jbc.273.32.20390.

29. Laine, J.P., Opresko, P.L., Indig, F.E., Harrigan, J.A., von Kobbe, C., and Bohr, V.A. (2003). Werner protein stimulates topoisomerase I DNA relaxation activity. Cancer Res. *63*, 7136–7146.

30. Goswami, A., Qiu, S., Dexheimer, T.S., Ranganathan, P., Burikhanov, R., Pommier, Y., and Rangnekar, V.M. (2008). Par-4 binds to topoisomerase 1 and attenuates its DNA relaxation activity. Cancer Res. *68*, 6190–6198. https://doi.org/10.1158/0008-5472.CAN-08-0831.

31. Pourquier, P., Ueng, L.M., Kohlhagen, G., Mazumder, A., Gupta, M., Kohn, K.W., and Pommier, Y. (1997). Effects of uracil incorporation, DNA mismatches, and abasic sites on cleavage and religation activities of mammalian topoisomerase I. J. Biol. Chem. *272*, 7792–7796. https://doi.org/10.1074/jbc.272.12.7792.

32. Baltz, A.G., Munschauer, M., Schwanhäusser, B., Vasile, A., Murakawa, Y., Schueler, M., Youngs, N., Penfold-Brown, D., Drew, K., Milek, M., et al. (2012). The mRNA-bound proteome and its global occupancy profile on protein-coding transcripts. Mol. Cell *46*, 674–690. https://doi.org/10.1016/j.molcel.2012.05.021.

33. Castello, A., Fischer, B., Eichelbaum, K., Horos, R., Beckmann, B.M., Strein, C., Davey, N.E., Humphreys, D.T., Preiss, T., Steinmetz, L.M., et al. (2012). Insights into RNA biology from an atlas of mammalian mRNA-binding proteins. Cell *149*, 1393–1406. https://doi.org/10.1016/j.cell.2012.04.031.

34. He, C., Sidoli, S., Warneford-Thomson, R., Tatomer, D.C., Wilusz, J.E., Garcia, B.A., and Bonasio, R. (2016). High-Resolution Mapping of RNA-Binding Regions in the Nuclear Proteome of Embryonic Stem Cells. Mol. Cell *64*, 416–430. https://doi.org/10.1016/j.molcel.2016.09.034.

35. Munschauer, M., Nguyen, C.T., Sirokman, K., Hartigan, C.R., Hogstrom, L., Engreitz, J.M., Ulirsch, J.C., Fulco, C.P., Subramanian, V., Chen, J., et al. (2018). The NORAD lncRNA assembles a topoisomerase complex critical for genome stability. Nature *561*, 132–136. https://doi.org/10.1038/s41586-018-0453-z.

36. Caudron-Herger, M., Rusin, S.F., Adamo, M.E., Seiler, J., Schmid, V.K., Barreau, E., Kettenbach, A.N., and Diederichs, S. (2019). R-DeeP: Proteome-wide and Quantitative Identification of RNA-Dependent Proteins by Density Gradient Ultracentrifugation. Mol. Cell *75*, 184–199.e10. https://doi.org/10.1016/j.molcel.2019.04.018.

37. Abe, K., Maunze, B., Lopez, P.A., Xu, J., Muhammad, N., Yang, G.Y., Katz, D., Liu, Y., and Lauberth, S.M. (2024). Downstream-of-gene (DoG) transcripts contribute to an imbalance in the cancer cell transcriptome. Sci. Adv. *10*, eadh9613. https://doi.org/10.1126/sciadv.adh9613.

38. Tan, Y., Yao, L., Gamliel, A., Nair, S.J., Taylor, H., Ohgi, K., Aggarwal, A.K., and Rosenfeld, M.G. (2023). Signal-induced enhancer activation requires Ku70 to read topoisomerase1–DNA covalent complexes. Nat. Struct. Mol. Biol. *30*, 148–158. https://doi.org/10.1038/s41594-022-00883-8.

39. Rahnamoun, H., Lu, H., Duttke, S.H., Benner, C., Glass, C.K., and Lauberth, S.M. (2017). Mutant p53 shapes the enhancer landscape of cancer cells in response to chronic immune signaling. Nat. Commun. *8*, 754. https://doi.org/10.1038/s41467-017-01117-y.

40. Restle, A., Färber, M., Baumann, C., Böhringer, M., Scheidtmann, K.H., Müller-Tidow, C., and Wiesmüller, L. (2008). Dissecting the role of p53 phosphorylation in homologous recombination provides new clues for gain-of-function mutants. Nucleic Acids Res. *36*, 5362–5375. https://doi.org/10.1093/nar/gkn503.

41. Albor, A., Kaku, S., and Kulesz-Martin, M. (1998). Wild-type and mutant forms of p53 activate human topoisomerase I: a possible mechanism for gain of function in mutants. Cancer Res. *58*, 2091–2094.

42. Szklarczyk, D., Gable, A.L., Nastou, K.C., Lyon, D., Kirsch, R., Pyysalo, S., Doncheva, N.T., Legeay, M., Fang, T., Bork, P., et al. (2021). The STRING database in 2021: customizable protein-protein networks, and functional characterization of user-uploaded gene/measurement sets. Nucleic Acids Res. *49*, D605–D612. https://doi.org/10.1093/nar/gkaa1074.

43. Van Nostrand, E.L., Pratt, G.A., Shishkin, A.A., Gelboin-Burkhart, C., Fang, M.Y., Sundararaman, B., Blue, S.M., Nguyen, T.B., Surka, C., Elkins, K., et al. (2016). Robust transcriptome-wide discovery of RNA-binding protein binding sites with enhanced CLIP (eCLIP). Nat. Methods *13*, 508–514. https://doi.org/10.1038/nmeth.3810.

44. Mo, Y.Y., Yu, Y., Shen, Z., and Beck, W.T. (2002). Nucleolar delocalization of human topoisomerase I in response to topotecan correlates with sumoylation of the protein. J. Biol. Chem. *277*, 2958–2964. https://doi.org/10.1074/jbc.M108263200.

45. Rallabhandi, P., Hashimoto, K., Mo, Y.Y., Beck, W.T., Moitra, P.K., and D'Arpa, P. (2002). Sumoylation of topoisomerase I is involved in its partitioning between nucleoli and nucleoplasm and its clearing from nucleoli in response to camptothecin. J. Biol. Chem. *277*, 40020–40026. https://doi.org/10.1074/jbc.M200388200.

46. Yung, T.M., Sato, S., and Satoh, M.S. (2004). Poly(ADP-ribosyl)ation as a DNA damage-induced post-translational modification regulating poly(ADP-ribose) polymerase-1-topoisomerase I interaction. J. Biol. Chem. *279*, 39686–39696. https://doi.org/10.1074/jbc.M402729200.

47. Kuleshov, M.V., Jones, M.R., Rouillard, A.D., Fernandez, N.F., Duan, Q., Wang, Z., Koplev, S., Jenkins, S.L., Jagodnik, K.M., Lachmann, A., et al. (2016). Enrichr: a comprehensive gene set enrichment analysis web server 2016 update. Nucleic Acids Res. *44*, W90–W97. https://doi.org/10.1093/nar/gkw377.

48. Nitiss, J.L., Soans, E., Rogojina, A., Seth, A., and Mishina, M. (2012). Topoisomerase assays. Curr. Protoc. Pharmacol. *Chapter 3*, Unit3.3. https://doi.org/10.1002/0471141755.ph0303s57.

49. Yan, J., Skoko, D., and Marko, J.F. (2004). Near-field-magnetic-tweezer manipulation of single DNA molecules. Phys. Rev. E Stat. Nonlin. Soft Matter Phys. *70*, 011905. https://doi.org/10.1103/PhysRevE.70.011905.

50. Skoko, D., Wong, B., Johnson, R.C., and Marko, J.F. (2004). Micromechanical analysis of the binding of DNA-bending proteins HMGB1, NHP6A, and HU reveals their ability to form highly stable DNA-protein complexes. Biochemistry *43*, 13867–13874. https://doi.org/10.1021/bi048428o.

51. Gunn, K.H., Marko, J.F., and Mondragón, A. (2018). Single-Molecule Magnetic Tweezer Analysis of Topoisomerases. Methods Mol. Biol. *1703*, 139–152. https://doi.org/10.1007/978-1-4939-7459-7_10.

52. Tabuchi, H., Handa, H., and Hirose, S. (1993). Underwinding of DNA on binding of yeast TFIID to the TATA element. Biochem. Biophys. Res. Commun. *192*, 1432–1438. https://doi.org/10.1006/bbrc.1993.1576.

53. Oksuz, O., Henninger, J.E., Warneford-Thomson, R., Zheng, M.M., Erb, H., Vancura, A., Overholt, K.J., Hawken, S.W., Banani, S.F., Lauman, R., et al. (2023). Transcription factors interact with RNA to regulate genes. Mol. Cell *83*, 2449–2463.e13. https://doi.org/10.1016/j.molcel.2023.06.012.

54. Drlica, K. (1992). Control of bacterial DNA supercoiling. Mol. Microbiol. *6*, 425–433. https://doi.org/10.1111/j.1365-2958.1992.tb01486.x.

55. Ma, J., Bai, L., and Wang, M.D. (2013). Transcription under torsion. Science *340*, 1580–1583. https://doi.org/10.1126/science.1235441.

56. Johnstone, C.P., and Galloway, K.E. (2022). Supercoiling-mediated feedback rapidly couples and tunes transcription. Cell Rep. *41*, 111492. https://doi.org/10.1016/j.celrep.2022.111492.

57. Avila-Lopez, P., and Lauberth, S.M. (2024). Exploring new roles for RNA-binding proteins in epigenetic and gene regulation. Curr. Opin. Genet. Dev. *84*, 102136. https://doi.org/10.1016/j.gde.2023.102136.

58. Wei, C., Xiao, R., Chen, L., Cui, H., Zhou, Y., Xue, Y., Hu, J., Zhou, B., Tsutsui, T., Qiu, J., et al. (2016). RBFox2 Binds Nascent RNA to Globally Regulate Polycomb Complex 2 Targeting in Mammalian Genomes. Mol. Cell *62*, 875–889. https://doi.org/10.1016/j.molcel.2016.04.013.

59. Barshad, G., Lewis, J.J., Chivu, A.G., Abuhashem, A., Krietenstein, N., Rice, E.J., Ma, Y., Wang, Z., Rando, O.J., Hadjantonakis, A.K., et al. (2023). RNA polymerase II dynamics shape enhancer-promoter interactions. Nat. Genet. *55*, 1370–1380. https://doi.org/10.1038/s41588-023-01442-7.

60. Core, L., and Adelman, K. (2019). Promoter-proximal pausing of RNA polymerase II: a nexus of gene regulation. Genes Dev. *33*, 960–982. https://doi.org/10.1101/gad.325142.119.

61. Christensen, M.O., Barthelmes, H.U., Feineis, S., Knudsen, B.R., Andersen, A.H., Boege, F., and Mielke, C. (2002). Changes in Mobility Account for Camptothecin-induced Subnuclear Relocation of Topoisomerase I*210. J. Biol. Chem. *277*, 15661–15665. https://doi.org/10.1074/jbc.C200066200.

62. Das, S.K., Rehman, I., Ghosh, A., SenGupta, S., Majumdar, P., Jana, B., and Das, B.B. (2016). Poly(ADP-ribose) polymers regulate DNA topoisomerase I (Top1) nuclear dynamics and camptothecin sensitivity in living cells. Nucleic Acids Res. *44*, 8363–8375. https://doi.org/10.1093/nar/gkw665.

63. Decker, C.J., Burke, J.M., Mulvaney, P.K., and Parker, R. (2022). RNA is required for the integrity of multiple nuclear and cytoplasmic membraneless RNP granules. EMBO J. *41*, e110137. https://doi.org/10.15252/embj.2021110137.

64. Davidovich, C., Wang, X., Cifuentes-Rojas, C., Goodrich, K.J., Gooding, A.R., Lee, J.T., and Cech, T.R. (2015). Toward a consensus on the binding specificity and promiscuity of PRC2 for RNA. Mol. Cell *57*, 552–558. https://doi.org/10.1016/j.molcel.2014.12.017.

65. Kaneko, S., Bonasio, R., Saldaña-Meyer, R., Yoshida, T., Son, J., Nishino, K., Umezawa, A., and Reinberg, D. (2014). Interactions between JARID2 and noncoding RNAs regulate PRC2 recruitment to chromatin. Mol. Cell *53*, 290–300. https://doi.org/10.1016/j.molcel.2013.11.012.

66. Cifuentes-Rojas, C., Hernandez, A.J., Sarma, K., and Lee, J.T. (2014). Regulatory interactions between RNA and polycomb repressive complex 2. Mol. Cell *55*, 171–185. https://doi.org/10.1016/j.molcel.2014.05.009.

67. Bose, D.A., Donahue, G., Reinberg, D., Shiekhattar, R., Bonasio, R., and Berger, S.L. (2017). RNA Binding to CBP Stimulates Histone Acetylation and Transcription. Cell *168*, 135–149.e22. https://doi.org/10.1016/j.cell.2016.12.020.

68. Rahnamoun, H., Lee, J., Sun, Z., Lu, H., Ramsey, K.M., Komives, E.A., and Lauberth, S.M. (2018). RNAs interact with BRD4 to promote enhanced chromatin engagement and transcription activation. Nat. Struct. Mol. Biol. *25*, 687–697. https://doi.org/10.1038/s41594-018-0102-0.

69. Pommier, Y. (2006). Topoisomerase I inhibitors: camptothecins and beyond. Nat. Rev. Cancer *6*, 789–802. https://doi.org/10.1038/nrc1977.

70. Palle, K., Pattarello, L., van der Merwe, M., Losasso, C., Benedetti, P., and Bjornsti, M.A. (2008). Disulfide cross-links reveal conserved features of DNA topoisomerase I architecture and a role for the N terminus in clamp closure. J. Biol. Chem. *283*, 27767–27775. https://doi.org/10.1074/jbc.M804826200.

71. Gunn, K.H., Marko, J.F., and Mondragón, A. (2018). Single-Molecule Magnetic Tweezer Analysis of Topoisomerases. In DNA Topoisomerases. Methods in Molecular Biology (Humana Press). https://doi.org/10.1007/978-1-4939-7459-7_10.

72. Langmead, B., Trapnell, C., Pop, M., and Salzberg, S.L. (2009). Ultrafast and memory-efficient alignment of short DNA sequences to the human genome. Genome Biol. *10*, R25. https://doi.org/10.1186/gb-2009-10-3-r25.

73. Ramírez, F., Dündar, F., Diehl, S., Grüning, B.A., and Manke, T. (2014). deepTools: a flexible platform for exploring deep-sequencing data. Nucleic Acids Res. *42*, W187–W191. https://doi.org/10.1093/nar/gku365.

74. Love, M.I., Huber, W., and Anders, S. (2014). Moderated estimation of fold change and dispersion for RNA-seq data with DESeq2. Genome Biol. *15*, 550. https://doi.org/10.1186/s13059-014-0550-8.

75. Andrews, S. (2010). FastQC: a quality control tool for high throughput sequence data. http://www.bioinformatics.babraham.ac.uk/projects/fastqc.

76. Liao, Y., Smyth, G.K., and Shi, W. (2014). featureCounts: an efficient general purpose program for assigning sequence reads to genomic features. Bioinformatics *30*, 923–930. https://doi.org/10.1093/bioinformatics/btt656.

77. Frankish, A., Carbonell-Sala, S., Diekhans, M., Jungreis, I., Loveland, J.E., Mudge, J.M., Sisu, C., Wright, J.C., Arnan, C., Barnes, I., et al. (2023). GENCODE: reference annotation for the human and mouse genomes in 2023. Nucleic Acids Res. *51*, D942–D949. https://doi.org/10.1093/nar/gkac1071.

78. Kim, D., Langmead, B., and Salzberg, S.L. (2015). HISAT: a fast spliced aligner with low memory requirements. Nat. Methods *12*, 357–360. https://doi.org/10.1038/nmeth.3317.

79. Robinson, J.T., Thorvaldsdóttir, H., Winckler, W., Guttman, M., Lander, E.S., Getz, G., and Mesirov, J.P. (2011). Integrative genomics viewer. Nat. Biotechnol. *29*, 24–26. https://doi.org/10.1038/nbt.1754.

80. Zhang, Y., Liu, T., Meyer, C.A., Eeckhoute, J., Johnson, D.S., Bernstein, B.E., Nusbaum, C., Myers, R.M., Brown, M., Li, W., et al. (2008). Model-based Analysis of ChIP-Seq (MACS). Genome Biol. *9*, R137. https://doi.org/10.1186/gb-2008-9-9-r137.

81. Ewels, P., Magnusson, M., Lundin, S., and Käller, M. (2016). MultiQC: summarize analysis results for multiple tools and samples in a single report. Bioinformatics *32*, 3047–3048. https://doi.org/10.1093/bioinformatics/btw354.

82. Li, H., Handsaker, B., Wysoker, A., Fennell, T., Ruan, J., Homer, N., Marth, G., Abecasis, G., and Durbin, R.; 1000 Genome Project Data Processing Subgroup (2009). The Sequence Alignment/Map format and SAMtools. Bioinformatics *25*, 2078–2079. https://doi.org/10.1093/bioinformatics/btp352.

83. Dobin, A., Davis, C.A., Schlesinger, F., Drenkow, J., Zaleski, C., Jha, S., Batut, P., Chaisson, M., and Gingeras, T.R. (2013). STAR: ultrafast universal RNA-seq aligner. Bioinformatics *29*, 15–21. https://doi.org/10.1093/bioinformatics/bts635.

84. Krueger, F., James, F., Ewels, P., Afyounian, E., and Schuster-Boeckler, B. (2021). Title: FelixKrueger/TrimGalore: v0.6.7. Zenodo. https://zenodo.org/records/5127899.

85. Paoletti, A.C., Parmely, T.J., Tomomori-Sato, C., Sato, S., Zhu, D., Conaway, R.C., Conaway, J.W., Florens, L., and Washburn, M.P. (2006). Quantitative proteomic analysis of distinct mammalian Mediator complexes using normalized spectral abundance factors. Proc. Natl. Acad. Sci. USA *103*, 18928–18933. https://doi.org/10.1073/pnas.0606379103.

86. Lauberth, S.M., Nakayama, T., Wu, X., Ferris, A.L., Tang, Z., Hughes, S.H., and Roeder, R.G. (2013). H3K4me3 interactions with TAF3 regulate preinitiation complex assembly and selective gene activation. Cell *152*, 1021–1036. https://doi.org/10.1016/j.cell.2013.01.052.

87. Schuijers, J., Manteiga, J.C., Weintraub, A.S., Day, D.S., Zamudio, A.V., Hnisz, D., Lee, T.I., and Young, R.A. (2018). Transcriptional Dysregulation of MYC Reveals Common Enhancer-Docking Mechanism. Cell Rep. *23*, 349–360. https://doi.org/10.1016/j.celrep.2018.03.056.

88. Milligan, J.F., Groebe, D.R., Witherell, G.W., and Uhlenbeck, O.C. (1987). Oligoribonucleotide synthesis using T7 RNA polymerase and synthetic DNA templates. Nucleic Acids Res. *15*, 8783–8798. https://doi.org/10.1093/nar/15.21.8783.

89. Aoi, Y., Takahashi, Y.-H., Shah, A.P., Iwanaszko, M., Rendleman, E.J., Khan, N.H., Cho, B.-K., Goo, Y.A., Ganesan, S., Kelleher, N.L., et al. (2021). SPT5 stabilization of promoter-proximal RNA polymerase II. Mol. Cell *81*, 4413–4424.e5. https://doi.org/10.1016/j.molcel.2021.08.006.

90. Fei, J., Ishii, H., Hoeksema, M.A., Meitinger, F., Kassavetis, G.A., Glass, C.K., Ren, B., and Kadonaga, J.T. (2018). NDF, a nucleosome-destabilizing factor that facilitates transcription through nucleosomes. Genes Dev. *32*, 682–694. https://doi.org/10.1101/gad.313973.118.

Please cite this article in press as: Bhola et al., RNA interacts with topoisomerase I to adjust DNA topology, Molecular Cell (2024), https://doi.org/10.1016/j.molcel.2024.07.032

STAR★METHODS

KEY RESOURCES TABLE

REAGENT or RESOURCE	SOURCE	IDENTIFIER
Antibodies		
β actin (C4)	Santa Cruz	Cat# sc47778; RRID: AB_626632
FLAG	Sigma-Aldrich	Cat# F3165; RRID: AB_259529
GFP	Sigma-Aldrich	Cat# G1544; RRID: AB_439690
Normal Rabbit IgG	Cell Signaling Technology	Cat# 2729; RRID: AB_1031062
Mouse IgG HRP Conjugate	Promega	Cat# W4021; RRID: AB_430834
Rabbit IgG HRP Conjugate	Promega	Cat# W4011; RRID: AB_430833
Rpb1 NTD (D8L4Y)	Cell Signaling Technology	Cat# 14958; RRID: AB_2687876
Spike-in antibody	Active Motif	Cat# 61686; RRID: AB_2737370
Topo I (C-21)	Santa Cruz	Cat# sc32736; RRID: AB_628382
Topoisomerase I [EPR5375]	Abcam	Cat# ab219735; RRID: AB_10861978
Bacterial and Virus Strains		
NEB® 5-alpha Competent *E. coli* Cells	New England Biolabs	Cat# C2987H
Rosetta (DE3) Competent *E. coli* Cells	Sigma-Aldrich	Cat# 70954
One Shot TOP10 Chemically Competent *E. coli* Cells	Thermo Fisher Scientific	Cat# C404003
Chemicals, Peptides, and Recombinant Proteins		
Digoxigenin	Roche	Cat# 11214667001
0.1% Formic acid	Thermo Fisher Scientific	Cat# 85170
Boric Acid	Thermo Fisher Scientific	Cat# A73-500
16% Paraformaldehyde Aqueous Solution	Electron Microscopy Sciences	Cat# 15710
2-mercaptoethanol	Sigma-Aldrich	Cat# M3148
3x FLAG Peptide	Sigma-Aldrich	Cat# F4799
5% Criterion TBE-Urea Polyacrylamide Gel	Bio-Rad	Cat# 3450086
10% Criterion TBE Polyacrylamide Gel	Bio-Rad	Cat# 3450053
Acetonitrile	Sigma-Aldrich	Cat# 34851
Agarose	Thermo Fisher Scientific	Cat# BP1356500
Amersham Protran® Premium Western blotting membranes, nitrocellulose	Cytiva	Cat# GE10600003
Anti-FLAG M2 Affinity Gel	Millipore	Cat# A2220
ATP	Roche	Cat# 11277057001
Benzonase	Sigma-Aldrich	Cat# E1014
Bio-Rad Protein Assay Dye Reagent Concentrate	Bio-Rad	Cat# 5000006
Biotin-11-CTP	PerkinElmer	Cat# NEL542001EA
Biotin-11-UTP	PerkinElmer	Cat# NEL543001EA
Bovine Serum Albumin	Thermo Fisher Scientific	Cat# BP9706
C18 desalting columns	Thermo Fisher Scientific	Cat# 89873
Camptothecin	Sigma-Aldrich	Cat# C9911
D(+)-Sucrose	Thermo Fisher Scientific	Cat# 177140010
Dimethyl sulfoxide (DMSO)	Sigma-Aldrich	Cat# 472301
DMEM, High Glucose	Gibco	Cat# 11965118
DNase I	New England Biolabs	Cat# M0303S
Drosophila spike-in chromatin	Active Motif	Cat# 53083
Disuccinimidyl glutarate (DSG)	ProteoChem	Cat# c1104
DTT [DL-Dithiothreitol]	Research Products International	Cat# D11000
Dynabeads M-270 Streptavidin	Invitrogen	Cat# 65305

(*Continued on next page*)

Please cite this article in press as: Bhola et al., RNA interacts with topoisomerase I to adjust DNA topology, Molecular Cell (2024), https://doi.org/10.1016/j.molcel.2024.07.032

Continued

REAGENT or RESOURCE	SOURCE	IDENTIFIER
Dynabeads MyOne Streptavidin C1	Invitrogen	Cat# 65002
Dynabeads Protein A	Invitrogen	Cat# 10002D
Protein A/G Magnetic Beads	Invitrogen	Cat# 88803
EDTA	BioPioneer	Cat# C0119
Ethidium bromide	Sigma-Aldrich	Cat# E8751
ExoSAP-IT PCR Product Cleanup Reagent	Applied Biosystems	Cat# 78201.1.ML
FastAP	Thermo Fisher Scientific	Cat# EF0651
Fetal Bovine Serum	Gibco	Cat# 26140079
Glycerol	Sigma-Aldrich	Cat# G5516
Glycine	Sigma-Aldrich	Cat# 50046
GTP	Roche	Cat# 11277057001
HEPES	Sigma-Aldrich	Cat# H3375
Hydrochloric acid	Sigma-Aldrich	Cat# 320331
IGEPAL® CA-630	Sigma-Aldrich	Cat# I8896
Iodoacetamide	Thermo Fisher Scientific	Cat# A39271
Lipofectamine 3000	Invitrogen	Cat# L3000015
Lithium chloride	Sigma-Aldrich	Cat# L9650
Magnesium chloride hexahydrate	Sigma-Aldrich	Cat# M2670
N-Lauroylsarcosine sodium salt	Sigma-Aldrich	Cat# 61745
NaOH	Thermo Fisher Scientific	Cat# S318500
Nonfat dry milk	Apex	Cat# 20-241
Open-Top Thinwall Ultra-Clear Tube	Beckman Coulter	Cat# 344060
PBS	Gibco	Cat# 10010049
Phenylmethanesulfonyl fluoride	Sigma-Aldrich	Cat# P7626
Pluronic F-127	Sigma-Aldrich	Cat# P2443
Polybrene	Sigma-Aldrich	Cat# TR1003
Potassium Chloride	Thermo Fisher Scientific	Cat# P2173
Potassium Hydroxide	Sigma-Aldrich	Cat# 484016
Potassium Acetate	Thermo Fisher Scientific	Cat# 013449.22
PhosStop	Roche	Cat# 4906845001
Protease Inhibitor Cocktail	Sigma-Aldrich	Cat# P8340
Proteinase K	MP Biomedicals	Cat# 193504
Protogel (30%) 37.5:1 Acrylamide to Bisacrylamide	National Diagnostics	Cat# EC8901LTR
Puromycin Dihydrochloride	Gibco	Cat# A1113803
Q5 High-Fidelity 2X Master Mix	New England Biolabs	Cat# M0492L
RapiGest SF reagent	Waters Corp	Cat# 186002122
Recombinant Albumin	New England Biolabs	Cat# B9200S
Ribonucleic Acid, Yeast	Millipore	Cat# 55714
RNA 5' Pyrophosphohydrolase (RppH)	New England Biolabs	Cat# M0356S
RNase I	Thermo Fisher Scientific	Cat# AM2294
RNaseOUT Recombinant Ribonuclease Inhibitor	Invitrogen	Cat# 10777019
Sodium Chloride	Thermo Fisher Scientific	Cat# S27110
Sodium deoxycholate	Sigma-Aldrich	Cat# D6750
Sodium dodecyl sulfate	Sigma-Aldrich	Cat# 74255
SuperScript IV	Invitrogen	Cat# 18090010
SuperSignal West Femto Maximum Sensitivity Substrate	Thermo Fisher Scientific	Cat# 34095
SYBR Gold Nucleic Acid Gel Stain	Invitrogen	Cat# S11494
Syringe Filter, Sterile, 0.45μm	Celltreat Scientific Products	Cat# 229749

(*Continued on next page*)

Please cite this article in press as: Bhola et al., RNA interacts with topoisomerase I to adjust DNA topology, Molecular Cell (2024), https://doi.org/10.1016/j.molcel.2024.07.032

Continued

REAGENT or RESOURCE	SOURCE	IDENTIFIER
Syringe Filters, Sterile, 0.22 μm	Celltreat	Cat# 229747
Spike-in chromatin	Active motif	Cat# 53083
T4 Polynucleotide Kinase	New England Biolabs	Cat# M0201L
T4 RNA ligase	New England Biolabs	Cat# M0437M
TCEP (Tris(2-carboxyethyl) phosphine	Thermo Fisher Scientific	Cat# J60316.09
Thermo Scientific Pierce ECL Western Blotting Substrate	Thermo Fisher Scientific	Cat# PI32209
Tris Base	Thermo Fisher Scientific	Cat# BP152
Triton X-100	Sigma-Aldrich	Cat# T9284
TRIzol reagent	Invitrogen	Cat# 15596026
Trypsin (0.25%), phenol red	Gibco	Cat# 15050065
Trypsin MS grade protease	Thermo Fisher Scientific	Cat# 90057
TWEEN® 20	Sigma-Aldrich	Cat# P1379
UltraPure Water	IBI Scientific	Cat# IB42200
UPLC BEH C18 Column	Waters Corp	Cat# 186002346
Urea	Sigma-Aldrich	Cat# U5128
Zinc Chloride	Sigma-Aldrich	Cat# 211273
γ-32P-ATP	PerkinElmer	Cat# BLU502H250UC
PEG 8000	Promega	Cat# V3011
Phenol:Chloroform:Isoamyl Alcohol mixture 25:24:1	Sigma-Aldrich	Cat# 77617
Ethanol, absolute (200 proof)	Thermo Fisher Scientific	Cat# BP2818100
Critical Commercial Assays		
7.5% Mini-PROTEAN	Bio-Rad	Cat# 4561024
Bio-Spin P-30 Columns	Bio-Rad	Cat# 7326231
D1000 ScreenTape	Agilent Technologies	Cat# 5067-5582
Direct-zol RNA Microprep	Zymo Research	Cat# R2062
ERCC RNA Spike-In Mix	Thermo Fisher Scientific	Cat# 4456740
Iblot 2 Transfer Stacks, PVDF, mini	Thermo Fisher Scientific	Cat# IB24002
Iblot 2 Transfer Stacks, PVDF, regular size	Thermo Fisher Scientific	Cat# IB24001
TruSeq® Stranded Total RNA Library Prep	Illumina	Cat# 20020596
SMARTer® Stranded Total RNA-Seq Kit V2 – Pico Input RNA Kit	Takara BioUSA	Cat# 634411
KAPA High Throughput Library Preparation Kit	Roche	Cat# 7961901001
KAPA HyperPrep Kit	Roche	Cat# KR0961
KAPA RNA HyperPrep Kit with RiboErase (HMR)	Roche	Cat# KK8560
KAPA SYBR® FAST	Roche	Cat# SFUKB
Microspin G-25 columns	GE Healthcare Life Sciences	Cat# 27532501
Octet High Precision Streptavidin (SA) biosensors	Sartorius	Cat# 18-5117
Octet High Precision Streptavidin 2.0 (SAX2) biosensors	Sartorius	Cat# 18-5136
Pierce Coomassie Brilliant Blue R-250 Dye	Thermo Fisher Scientific	Cat# 20278
Pierce C18 Tips, 10 μL bed	Thermo Fisher Scientific	Cat# 87782
Polybead® Amino Microspheres 3.00μm	Polysciences Inc	Cat# 17145-5
ProtoScript® II First Strand cDNA Synthesis Kit	New England Biolabs	Cat# E6560S
QIAquick PCR Purification Kit	Qiagen	Cat# 28106
Qubit 1X dsDNA HS Assay Kit	Thermo Fisher Scientific	Cat# Q33230
RNA ScreenTape	Agilent Technologies	Cat# 5067-5576
SYBR Green Master Mix	Thermo Fisher Scientific	Cat# 4309155

(*Continued on next page*)

Continued

REAGENT or RESOURCE	SOURCE	IDENTIFIER
T7 RiboMAX Express Large Scale RNA Production System	Promega	Cat# P1320
UPrep® Spin Columns	Genesee Scientific	Cat# 88-243C
ZR small-RNA page recovery kit	Zymo research	Cat# R1070
Deposited Data		
Unprocessed files	This paper; Mendeley Data	Mendeley Data: https://doi.org/10.17632/m6j25dkdkn.1
TOP1 eCLIP	This paper	NCBI GEO: GSE213403
TOP1 UV-RIP-seq	This paper	NCBI GEO: GSE213403
TOP1cc-seq	Abe et al.[37]	NCBI GEO: GSE202408
PRO-seq	Abe et al.[37]	NCBI GEO: GSE202408
GFP-TOP1cc-seq for TOP1 WT	This paper	NCBI GEO: GSE213403
GFP-TOP1cc-seq for TOP1 ΔRBR	This paper	NCBI GEO: GSE213403
H3K27ac ChIP-seq	Rahnamoun et al.[39]	NCBI GEO: GSE102796
H3K4me1 ChIP-seq	Rahnamoun et al.[39]	NCBI GEO: GSE102796
Experimental Models: Cell Lines		
Human: HCT116	ATCC	Cat# CCL-247; RRID: CVCL_0291
Human: HEK293T	ATCC	Cat# CRL-3216; RRID: CVCL_0063
Human: SW480	ATCC	Cat# CCL-228; RRID: CVCL_0546
Oligonucleotides		
RT-qPCR and ChIP-qPCR primers, in vitro RNA synthesis primers, EMSA probes and primers, and shRNA oligonucleotides	This paper	See Table S4
Recombinant DNA		
pcDNA3.1	Invitrogen	Cat# V79020
pFOS1	Alfonso Mondragon Lab[71]	N/A
pIsotRNA.Mt	Alfonso Mondragon Lab[71]	N/A
pUC19	Alfonso Mondragon Lab[71]	N/A
pLKO.1 TRC LacZ control	Lauberth lab[68]	N/A
pLKO.1 TRC shTOP1-3'UTR	Lauberth lab[37]	N/A
pMD2.G	pMD2.G was a gift from Didier Trono	Addgene plasmid Cat# 12259; http://n2t.net/addgene:12259; RRID:Addgene_12259
psPAX2	psPAX2 was a gift from Didier Trono	Addgene plasmid Cat# 12260; http://n2t.net/addgene:12260; RRID:Addgene_12260
GFP-FLAG-TOP1-WT	This paper	GENEWIZ
GFP-FLAG-TOP1-ΔRBR	This paper	GENEWIZ
Software and Algorithms		
Adobe acrobat (illustrator for manuscript preparation)	Adobe	https://www.adobe.com
BLItz Pro software (version 1.1.0.31)	ForteBio	N/A
Bowtie2 v2.4.5	Langmead et al.[72]	https://bowtie-bio.sourceforge.net/bowtie2/index.shtml
Deeptools v3.5.1	Ramírez et al.[73]	https://github.com/deeptools/deepTools
DESeq2 v1.38.3	Love et al.[74]	https://bioconductor.org/packages/release/bioc/html/DESeq2.html
Enrichr	Kuleshov et al.[47]	https://maayanlab.cloud/Enrichr/
FastQC	Andrews.[75]	https://www.bioinformatics.babraham.ac.uk/projects/fastqc/

(*Continued on next page*)

Please cite this article in press as: Bhola et al., RNA interacts with topoisomerase I to adjust DNA topology, Molecular Cell (2024), https://doi.org/10.1016/j.molcel.2024.07.032

Continued

REAGENT or RESOURCE	SOURCE	IDENTIFIER
featureCounts v2.0.3	Liao et al.[76]	https://subread.sourceforge.net/featureCounts.html
GENCODE v45	Frankish et al.[77]	https://www.gencodegenes.org/
GraphPad Prism 9	GraphPad Software	https://www.graphpad.com/
HISAT2 v2.2.1	Kim et al.[78]	https://daehwankimlab.github.io/hisat2/
IGV genome browser v.2.16.1	Robinson et al.[79]	http://software.broadinstitute.org/software/igv/
ImageLab Software 6.1	Bio-Rad	N/A
MACS2 v2.1.1, v3.0.0	Zhang et al.[80]	N/A
MultiQC	Ewels et al.[81]	https://multiqc.info/
PMI-Byonic (PMI) version 2.9.30	Protein Metrics by Dotmatics	https://proteinmetrics.com/byonic/
PyBigWig	PyPI	https://github.com/deeptools/pyBigWig
RBR-ID	He et al.[34]; Oksuz et al.[53]	http://rbrid.bonasiolab.org/rbrid/
SAMtools v1.6	Li et al.[82]	https://samtools.sourceforge.net/
STAR v2.7.5	Dobin et al.[83]	https://github.com/alexdobin/STAR
TrimGalore	Krueger et al.[84]	https://github.com/FelixKrueger/TrimGalore

RESOURCE AVAILABILITY

Lead contact

Further information and requests for resources and reagents should be directed to and will be fulfilled by the lead contact, Shannon Lauberth (shannon.lauberth@northwestern.edu).

Materials availability

Reagents generated in this study are available upon request from the lead contact and will be shared via a materials transfer agreement.

Data and code availability

- eCLIP, UV-RIP-seq and TOP1cc-seq data is publicly available at GEO: GSE213403.
- This paper does not report original code.
- Any additional information required to reanalyze the data reported in this paper is available from the lead contact upon request.

EXPERIMENTAL MODEL AND STUDY PARTICIPANT DETAILS

Cell Culture and Treatments

Human colorectal adenocarcinoma SW480, HCT116, and human embryonic kidney 293T (HEK293T) cells were purchased from the American Type Culture Collection (ATCC) and grown in Dulbecco's modified Eagle medium (DMEM, Gibco) supplemented with 10% fetal bovine serum (FBS, Gibco). Lentivirus infected SW480 cells were propagated in growth medium containing DMEM, 10% FBS, and 1.5 μg/mL puromycin. The cell lines were grown in a 37°C incubator supplied with 5% CO_2. All cell lines tested negative for mycoplasma contamination by PCR.

Lentivirus Production and Transduction

pLKO.1 TRC control and target shRNA plasmids were generated with annealed primers to knockdown TOP1. shRNA primers used in this study are listed in Table S4. For lentivirus production and transduction, 50–60% confluent HEK293T cells were transfected with Lipofectamine 3000 (Invitrogen) with TRC control, target shRNAs, and packaging plasmids psPAX2 and pMD2.G. Virus-containing medium was collected 48 and 72 h post transfection, filtered with a 0.45-μm pore size filter, and used for viral infection. SW480 cells were transduced with viral supernatants containing 8 μg/mL polybrene (Sigma-Aldrich). After 8 h infection, virus-containing medium was removed and replaced with fresh medium. After 48 h, puromycin was added at a final concentration of 1.5 μg/mL. Cells were cultured for an additional 8 days before harvesting the cells for RT-qPCR and immunoblot to confirm successful knockdown efficiency.

SW480 cells stably expressing TOP1 shRNAs were transfected with empty vector, GFP-FLAG-TOP1 WT or GFP-FLAG-TOP1 ΔRBR using Lipofectamine 3000 (Invitrogen) according to the manufacturer's directions (Life Technologies). Cells were harvested 48h post-transfection for immunoblot, UV-RIP-qPCR, Co-IP, and TOP1-seq.

Please cite this article in press as: Bhola et al., RNA interacts with topoisomerase I to adjust DNA topology, Molecular Cell (2024), https://doi.org/10.1016/j.molcel.2024.07.032

METHOD DETAILS

Antibodies

Antibodies used for TOP1cc-seq, eCLIP, Co-IP, and UV-RIP analyses were obtained commercially and are as follows: anti-TOP1 (abcam, ab219735, 2μg), anti-Spike-in antibody (Active Motif, 61686, 1 μg), anti-IgG (Cell Signaling, 2729S, 2μg), anti-FLAG (Sigma, F3165, 2μg), and anti-GFP (Sigma, G1544, 2 μg. Antibodies used for immunoblotting are as follows: anti-β actin (Santa Cruz, sc47778, 1:1000 dilution), anti-TOP1 (Santa Cruz, sc-32736, 1:1000 dilution), anti-FLAG (Sigma, F3165, 1:1000 dilution), anti-Rpb1 NTD (D8L4Y) (Cell Signaling, 14958, 1:1000 dilution), and anti-GFP (Sigma, G1544, 1:1000 dilution). Secondary antibodies used for immunoblotting include Mouse IgG HRP Conjugate (Promega, W402B, 1:3000), Rabbit IgG HRP Conjugate (Promega, W4011, 1:5000).

Immunoblotting

Protein samples were incubated at 95°C for 5 min, separated by SDS-PAGE, and transferred to PVDF membranes (Invitrogen). The membranes were blocked in 3% milk and probed with the indicated antibodies. Reactive bands were detected by Pierce ECL Plus (Thermo Scientific Pierce) or SuperSignal West Femto (Thermo Scientific Pierce) and visualized using the Odyssey Fc Imaging System (LI-COR Biosciences) or the ChemiDoc Imaging system (Bio-Rad Laboratories).

RNA Purification and RT-qPCR

Total RNA was extracted with TRIzol reagent (Invitrogen) following manufacturer's instructions. Total RNA was used for cDNA synthesis using the ProtoScript II First Strand cDNA Synthesis Kit (NEB) with random hexamers. qPCR reactions were performed using SYBR Green PCR Master Mix (Applied Biosystems) on an Applied Biosystems QuantStudio3 real-time PCR system in triplicate using samples from three independent cell harvests. The specificity of amplification was confirmed by melting curve analysis. The relative levels of eRNA and mRNA expression were calculated using the (ΔΔCt) method and individual expression data was normalized to *GAPDH*. Primers for RT-qPCR are listed in Table S4.

Sucrose Density Gradient Ultracentrifugation

Sucrose density gradient ultracentrifugation assays were performed following previously established protocols[36] with minor modifications. To prepare the sucrose density gradient, 1 mL sucrose solutions from 50% (w/v) to 5% in 10 mM Tris-HCl pH 7.5, 100 mM NaCl, and 1 mM EDTA were filtered with a 0.22-μm pore size filter and layered on top of each other in ultra-clear tubes (Beckman Coulter) with the 50% sucrose solution on the bottom. Each layer was frozen at -80°C for 15 min before the addition of the next layer. Prepared sucrose gradients were stored at -20°C and slowly thawed at 4°C for one hour prior to starting centrifugation.

SW480 cells were lysed in 20 mM Tris-HCl pH 7.5, 300 mM NaCl, 2 mM EDTA, 0.5% NP40, 1% Triton X-100, 1 mM PMSF, PICs and incubated on ice for 30 min with gentle vortexing every 5 min. Lysates were cleared by centrifugation at 14,000 rpm for 10 min at 4°C and protein concentration was determined using bovine serum albumin (BSA) standard. Two milligrams of cleared lysates were gently layered on top of the sucrose gradient without perturbing the layers. Centrifugation was performed using a Beckman ultracentrifuge with an SW40 Ti swinging bucket rotor at 30,000 rpm for 18 h at 4°C. Following ultracentrifugation, gradient tubes were removed from the rotor without disturbing the layers and starting from the top, 25 fractions of 400 μL each were collected into fresh 1.5 mL tubes and 5% of each fraction was analyzed by TOP1 immunoblot analysis.

TOP1 IP Followed by Mass Spectrometry

Following TOP1 immunoblot analysis, sucrose gradient fractions with the highest levels of TOP1 protein were pooled together (Fractions 20-25). Pooled fractions were diluted two-fold with 10 mM Tris-HCl pH 7.5, 100 mM NaCl, and 1 mM EDTA. Protein A Dynabeads (Invitrogen) pre-coupled with TOP1 or IgG antibodies were subsequently used for IP from the pooled sucrose fractions overnight at 4°C. Immunocomplexes were washed three times in ice-cold wash buffer (50 mM Tris-HCl pH 7.4, 150 mM NaCl, 0.5% sodium deoxycholate, 1% SDS, 0.1% NP-40) and three times in 1X PBS. After the removal of the last PBS wash, protein-bound beads were either denatured at 70°C for 10 min for SDS-PAGE or frozen at -80°C for storage prior to mass-spectrometry analysis by the Biomolecular and Proteomics Mass Spectrometry Facility, University of California San Diego.

Mass Spectrometry

Protein samples were diluted in TNE buffer (50 mM Tris pH 8.0, 100 mM NaCl, 1 mM EDTA). RapiGest SF reagent (Waters Corp) was added to the mix to a final concentration of 0.1% and samples were boiled for 5 min. TCEP (Tris (2-carboxyethyl) phosphine) was added to 1 mM (final concentration) and the samples were incubated at 37°C for 30 min. Subsequently, the samples were carboxymethylated with 0.5 mg/ml of iodoacetamide for 30 min at 37°C followed by neutralization with 2 mM TCEP (final concentration). Protein samples prepared as above were digested with trypsin (trypsin:protein ratio - 1:50) overnight at 37°C. RapiGest was degraded and removed by treating the samples with 250 mM HCl at 37°C for 1 h followed by centrifugation at 14,000 rpm for 30 min at 4°C. The soluble fraction was then added to a new tube and the peptides were extracted and desalted using C18 desalting columns (Thermo Scientific). Peptides were quantified using BCA assay and a total of 1 μg of peptides were injected for LC-MS analysis.

Please cite this article in press as: Bhola et al., RNA interacts with topoisomerase I to adjust DNA topology, Molecular Cell (2024), https://doi.org/10.1016/j.molcel.2024.07.032

Trypsin-digested peptides were analyzed by ultra-high pressure liquid chromatography (UPLC) coupled with tandem mass spectroscopy (LC-MS/MS) using nano-spray ionization. The nanospray ionization experiments were performed using a Orbitrap fusion Lumos hybrid mass spectrometer (Thermo) interfaced with nanoscale reversed-phase UPLC (Thermo Dionex UltiMate 3000 RSLC nano System) using a 25 cm, 75-micron ID glass capillary packed with 1.7-μm C18 BEHTM beads (Waters corporation). Peptides were eluted from the C18 column into the mass spectrometer using a linear gradient (5–80%) of ACN (Acetonitrile) at a flow rate of 375 μL/min for 1h. The Buffer A (98% H2O, 2% ACN, 0.1% formic acid) and Buffer B (100% ACN, 0.1% formic acid) were used to create the ACN gradient. Mass spectrometer parameters are as follows; an MS1 survey scan using the orbitrap detector (mass range (m/z): 400-1,500 (using quadrupole isolation), 120,000 resolution setting, spray voltage of 2200 V, Ion transfer tube temperature of 275°C, AGC target of 400,000, and maximum injection time of 50 ms) was followed by data dependent scans (top speed for most intense ions, with charge state set to only include +2-5 ions, and 5 second exclusion time, while selecting ions with minimal intensities of 50,000 at in which the collision event was carried out in the high energy collision cell (HCD Collision Energy of 30%), and the fragment masses where analyzed in the ion trap mass analyzer (with ion trap scan rate of turbo, first mass m/z was 100, AGC Target 5000 and maximum injection time of 35ms). Protein identification was carried out using PMI-Byonic (PMI) version 2.9.30. The NSF calculations were carried out using Perl scripts based on the calculations described by Paoletti et al.[85] A Second Perl script was used to align all data from all samples into a single table.

Enhanced Crosslinking IP (eCLIP)

eCLIP was performed as described.[43] In brief, SW480 cells (20×10^6) were UV crosslinked (400 mJ/cm^{-2} at 254 nm) and saved at -80°C until processing. Briefly, cells were lysed in CLIP lysis buffer (50 mM Tris-HCl, pH 7.4, 100 mM NaCl, 1% NP40, 0.1% SDS, 0.5% sodium deoxycholate) and sonicated (BioRuptor). Following the fragmentation of RNA with RNase I (Ambion), TOP1 (Abcam, ab219735) and rabbit IgG (Cell Signaling, 2729S) protein-RNA complexes were immunoprecipitated using the indicated antibodies. Stringent washes were performed using wash buffer (50 mM Tris-HCl, pH 7.4, 1 M NaCl, 1 mM EDTA, 1% NP-40, 0.1% SDS, 0.5% sodium deoxycholate). RNA was dephosphorylated using FastAP (Fisher Scientific) and T4 PNK (NEB). Subsequently, a 3' RNA adaptor was ligated onto the RNA with T4 RNA ligase (NEB). TOP1-RNA complexes were separated by SDS-PAGE, transferred to a nitrocellulose membrane, and RNA was extracted from the membrane using proteinase K (NEB). Following precipitation, RNA was reverse transcribed with Superscript IV (Invitrogen), free primer was removed (ExoSap-IT, Affymetrix) and a 3' DNA adaptor was ligated onto the cDNA product with T4 RNA ligase (NEB). Complementary DNA was amplified by PCR using Q5 Master Mix (NEB) and purified before Illumina sequencing. In addition to the RBP immunoprecipitations, parallel size-matched input libraries were generated to aid in the removal of false positives. A library was also generated from RNAs bound to IgG to normalize nonspecific binding. Libraries for eCLIP samples were sequenced by Admera Health.

Ultraviolet-RNA Immunoprecipitation (UV-RIP)

SW480 cells were crosslinked by UV irradiation (150 mJ/cm^{-2} at 254 nm) using CL-3000 UV Crosslinker (Analytik Jena). The cells were lysed in RIP lysis buffer [25 mM HEPES-KOH pH 7.5, 150 mM KCl, 0.5% NP40, 1.5 mM $MgCl_2$, 10% glycerol, 1mM EDTA, 0.4 U RNaseOUT (Thermo Fisher Scientific), protease inhibitor cocktails (PICs)] on ice for 30 min. Cleared lysates were immunoprecipitated overnight with Protein A Dynabeads (Invitrogen) pre-coupled to TOP1 and IgG antibodies. Cleared lysates prepared from SW480 cells transiently expressing EV, GFP-FLAG-TOP1 WT or GFP-FLAG-TOP1 ΔRBR were immunoprecipitated with GFP antibody precoupled Protein A dynabeads (Sigma). Beads were subsequently washed three times with RIP lysis buffer and RNA samples were eluted using TRIzol reagent (Invitrogen).

For UV-RIP-seq, RNA was extracted using TRIzol (Invitrogen) as described above. Briefly, RNA sample quality was assessed by High Sensitivity RNA Tapestation (Agilent Technologies Inc., California, USA) and quantified by Qubit 2.0 RNA HS assay (ThermoFisher, Massachusetts, USA). Library construction is performed based on manufacturer's recommendation for SMARTer® Stranded Total RNA-Seq Kit V2 – Pico Input RNA Kit (Takara Bio USA Inc., California, USA) with ERCC RNA spike-in Mix (ThermoFisher, Massachusetts, USA). Final library quantity was measured by KAPA SYBR® FAST qPCR and library quality evaluated by TapeStation D1000 ScreenTape (Agilent Technologies, CA, USA). Final library size ranges from 300-400 bp with Illumina® 8-nt dual-indices were used. Equimolar pooling of libraries was performed based on QC values and sequenced on an Illumina® NovaSeq S4 (Illumina, California, USA) with a read length configuration of 150 PE for 50M reads per sample (25M in each direction). NGS Libraries were generated and sequenced by Admera Health.

For UV-RIP-qPCR, RNA and cDNA samples were prepared as described above and analyzed by RT-qPCR primers listed in Table S4.

Purification of Recombinant TOP1 Full Length Protein

The TOP1 full length protein was previously purified on FLAG resin (Sigma) following expression from the pFAST-BAC1 vector in Sf9 cells as described.[86]

In Vitro RNA synthesis

Primers were designed to amplify desired genomic regions that correspond to the RNA sequence enriched in the TOP1 UV-RIP and eCLIP experiments and with the RNA signal confirmed by (PRO-seq) at *45s* rRNA, *PNP* mRNA, *ACSL1* mRNA, *MYC* eRNA, *MMP9*

Please cite this article in press as: Bhola et al., RNA interacts with topoisomerase I to adjust DNA topology, Molecular Cell (2024), https://doi.org/10.1016/j.molcel.2024.07.032

eRNA, and *CCL2* eRNA. The *MYC* enhancer location was identical to that previously described.[87] The T7 promoter sequence was included in the forward primer and genomic fragments PCR amplified from SW480 cDNA, confirmed by sequencing, and subsequently used for RNA synthesis using T7 RiboMAX Express Large-Scale RNA Production System (Promega) per the manufacturer's instructions. The synthesized RNAs were then purified with MicroSpin G-25 Columns (GE Healthcare Life Sciences), quantitated by Nanodrop (Invitrogen), and verified on a 5% TBE urea gel followed by staining with SYBR Gold (Life Technologies) for 20 min prior to imaging using LI-COR Odyssey Fc Imaging System. To generate the *PNP* dsRNA, the T7 promoter sequence was added to the forward and reverse primer. Full-length *Mycobacterium tuberculosis* $tRNA^{Ile}$ was produced *in vitro* by run-off transcription using recombinant T7 RNA polymerase and standard reaction conditions.[88] In brief, the DNA template encoding *M. tuberculosis* $tRNA^{Ile}$ was cloned into the multiple cloning site of pUC19 with an upstream T7 RNA polymerase promoter element and a BsmI restriction site immediately 3' to the coding region. Plasmid DNA was transformed into *E. coli* DH5α, grown in Luria-Bertani medium, purified by conventional alkaline lysis methods and phenol-chloroform extracted and selective PEG 8000 precipitated to remove contaminating cellular host proteins and RNAs, respectively. The purified plasmid DNA was subsequently digested with BsmI (New England BioLabs) and purified further by phenol-chloroform extraction and ethanol precipitation. Following *in vitro* transcription, *M. tuberculosis* $tRNA^{Ile}$ was separated from short transcripts and other reaction components by electrophoresis in a native 10% acrylamide gel in 1X TB buffer (89 mM Tris-HCl, pH 7.6, 89 mM boric acid). The principal gel band corresponding to the *M. tuberculosis* $tRNA^{Ile}$ transcription product was located by UV shadowing and extracted into 50 mM potassium acetate, pH 7.0, 200 mM potassium chloride by passive diffusion at 4°C. The extracted RNAs were both precipitated with ethanol and stored at -20°C.

The RNA probe sequences, and the primer sequences used for PCR amplification are listed in Table S4.

RNA Refolding

ssRNA and dsRNA *PNP* mRNA, *ACSL1* mRNA, *45s rRNA* and the *MYC*, *MMP9*, and *CCL2* eRNA probes were refolded by incubating the RNA at 85°C for 2 min followed by snap-cooling on an ice-cold metal rack for 5 min. The RNA was diluted 10-fold by adding pre-chilled RNA refolding buffer (10 mM Tris-HCl pH 7, 10 mM $MgCl_2$, 100 mM KCl), and the RNAs were allowed to refold by bringing the samples to room temperature for 30 min, prior to performing the binding assays. The tRNA was resuspended in tRNA refolding buffer (10 mM HEPES pH 7.0, 50 mM NaCl) and incubated at 95°C for 3 min. The RNA was then incubated on ice for 3 min. prior to adding $MgCl_2$ to a final concentration of 15 mM. The tRNA was then incubated for an additional 10 min at 50°C and then 37°C for another 30 min. Finally, the tRNA was incubated at room temperature for 10 min prior to the binding assays.

Electrophoretic Mobility Shift Assays

EMSAs were performed following established protocols with a few modifications.[68] Labeling reactions consisted of 10 pmol of DNA or 10 μg of RNA, T4 polynucleotide kinase (NEB) and γ-^{32}P-ATP (Perkin Elmer). Unincorporated γ-^{32}P-ATP was removed from DNA and RNA probes by purification with MicroSpin G-25 Columns (GE Healthcare Life Sciences) and extraction from 5% TBE urea gel using the ZR small-RNA PAGE Recovery Kit (Zymo Research), respectively. Labeled samples were quantified by running known amounts of unlabeled nucleic acid on an agarose gel for DNA or 5% TBE urea gel for RNA. Standard curves were generated following the quantification of the intensity of the nucleic acid bands using ImageJ. Binding reactions were performed using 1 nM of labeled RNA or DNA in 1X EMSA buffer [20 mM Tris-HCl pH 7.4, 100 mM KCl, 1mM EDTA, 1% glycerol, 0.05% NP40, 0.5 mM $ZnCl_2$, 0.1 mg/mL BSA (Fisher), 0.1 mg/mL yeast tRNA (Sigma), 2 mM DTT) and supplemented with 0.4U RNaseOUT (Thermo Fisher Scientific)] for RNA EMSAs. The RNA probe was refolded prior to its addition to the reaction as described above. The binding reactions were initiated by the addition of increasing concentrations of FLAG-TOP1 protein and incubation at 4°C for 30 min. Reactions were loaded on a 4% native polyacrylamide gel that was pre-chilled overnight and pre-run for 1 h at 150V. The gel was run for 4 h at 150V and exposed to an autoradiography screen for 12-16 h prior to imaging with a Typhoon phosphorimager.

In Vitro Pull-Down RNA binding assays

FLAG-tagged TOP1 protein was incubated with 0.33 μg of refolded RNA while rotating at 4°C for 1 h in RNA binding buffer [20 mM Tris-HCl at pH 7.4, 100 mM KCl, 0.2 mM EDTA, 0.05% NP40, 0.4 U RNaseOUT (Thermo Fisher Scientific), PICs]. Protein-RNA complexes were recovered using FLAG M2 agarose beads for 1h at 4°C. Beads were washed three times with RNA wash buffer [20 mM Tris-HCl at pH 7.4, 200 mM KCl, 0.2 mM EDTA, 0.05% NP40, 0.4 U RNaseOUT (Thermo Fisher Scientific), PICs] and RNA samples were eluted using TRIzol reagent (Invitrogen). Purified RNA samples were resolved on a denaturing 10% TBE urea gel and stained with SYBR Gold for 20 min before imaging using LI-COR Odyssey Fc Imaging System.

Biolayer-Interferometry (BLI) Assays

Sensorgrams were recorded on a FortéBio BLItz Interferometer using streptavidin (SA)-coated sensors. SAX and SAX2.0 sensors were used for RNA and DNA, respectively. Sensors were hydrated in binding buffer (300 mM KCl, 10% glycerol, 0.1 mM EDTA, 10 mM HEPES pH 7.6) for 10 min before 1 μM biotinylated and refolded *MYC* eRNA and dsDNA and *PNP* eRNA and dsDNA were immobilized in binding buffer on the SA sensor. Data was collected for varying amounts (0.10, 0.25, 0.50, 0.75, and 1.00 μM) of TOP1 protein. Injections of TOP1 protein were made with a 120 sec contact time and a 180 sec dissociation phase. All assays were performed at 25°C and with agitation at 2,600 rpm over the course of the experiment. The data were generated and analyzed

Please cite this article in press as: Bhola et al., RNA interacts with topoisomerase I to adjust DNA topology, Molecular Cell (2024), https://doi.org/10.1016/j.molcel.2024.07.032

by the BLItz Pro software (version 1.1.0.31) and figures were generated using R. The binding profile of each sample is summarized as a "nm shift" the wavelength/spectral shift in nanometers. The figures represent curves adjusted for the start of association and the start of dissociation as is done in the BLItz Pro software for analysis. The assays also generated a kinetic profile to characterize the binding affinities by determining both the on (ka) and off (kd) rates and the equilibrium dissociation constant (K_D), which was calculated by dividing the value of the ka into kd.

Co-Immunoprecipitation Assays

Co-Immunoprecipitation assays were performed as previously described with minor modifications.[89] SW480 cells transiently expressing empty vector, GFP-FLAG-TOP1 WT, or GFP-FLAG-TOP1 ΔRBR were resuspended in lysis buffer [10 mM Tris-HCl pH 7.4, 10 mM KCl, 1.5 mM MgCl2, 12% Sucrose, 10% Glycerol, 0.2% Triton X-100, 0.5 mM DTT, Phosphatase inhibitors (Roche), PICs (Sigma) and 1mM PMSF]. Then, the cell lysates were fractionated in sucrose cushion (10 mM Tris-HCl pH 7.4, 10 mM KCl, 1.5 mM MgCl2, 30% Sucrose, 0.5 mM DTT). Nuclei pellets were stored in freeze buffer (10 mM Tris-HCl pH 7.4, 10 mM KCl, 1.5 mM MgCl2, 40% Glycerol, 0.5 mM DTT) at -80°C.

Chromatin DNA/RNA was digested in Chromatin digestion buffer [20 mM Tris-HCl pH 7.4, 150 mM NaCl, 1.5 mM MgCl2, 10% Glycerol, 0.05% IGEPAL, 0.5 mM DTT, Protease inhibitors (Roche), 250 U/ml Benzonase (Sigma)]. After centrifuging at 20,000 x g for 5 minutes, the supernatant was collected as fraction 1. Proteins were further extracted from the pellet using a Chromatin-2 buffer (20 mM Tris-HCl pH 7.4, 500 mM NaCl, 1.5 mM MgCl2, 10% Glycerol, 0.05% IGEPAL, 0.5 mM DTT, Protease inhibitors PICs (Sigma), and 1mM PMSF, Phosphatase inhibitors (Roche), 3 mM EDTA), and collected as fraction 2. The NaCl concentration in fraction 2 was adjusted to 150 mM before combining it with fraction 1. TOP1 IP was performed using anti-Flag antibody (Sigma) conjugated to Protein A/G Magnetic Beads (Invitrogen). After washing three times with wash buffer (20 mM Tris-HCl pH 7.4, 225 mM NaCl, 1.5 mM MgCl2, 10% Glycerol, 1.5 mM EDTA, 0.05% IGEPAL, 0.5 mM DTT), immunoprecipitated proteins were eluted by boiling at 95°C for 5 min, separated by SDS-PAGE, and transferred to PVDF membranes (Invitrogen).

TOP1cc-Sequencing

The TOP1cc-seq methodology was adapted from a previously established protocol.[7] Briefly, SW480 cells transiently expressing EV, GFP-FLAG-TOP1 WT or GFP-FLAG-TOP1 ΔRBR were treated with 10 μM CPT for 4 min followed by immediate washing with ice-cold 1X PBS, scraped, and resuspended in lysis buffer (20 mM Tris-HCl pH 7.5, 300 mM NaCl, 2 mM EDTA, 0.5% NP40, 1% Triton X-100, 1 mM PMSF, PICs), and incubated on ice for 30 min. Cell resuspensions were next dounced ten times in a prechilled glass homogenizer. Nuclei were collected and resuspended in shearing buffer (0.1% SDS, 0.5% N-lauroylsarcosine, 1% Triton X-100, 10 mM Tris-HCl pH 8.1, 100 mM NaCl, 1 mM EDTA, 1 mM PMSF, PICs) and incubated on ice for 30 min. Chromatin was fragmented using an E220 Focused-Ultrasonicator (Covaris) to an average size of 200-600 bp. 0.2% spike-in chromatin (Active motif, 53083) was added to normalize out technical variation. The cleared chromatin was immunoprecipitated overnight at 4°C with Protein A Dynabeads that were pre-coupled in 0.5% BSA with IgG, TOP1, or GFP antibodies. Immunocomplexes were washed eight times in wash buffer (50 mM HEPES-KOH pH 7.6, 500 mM LiCl, 1 mM EDTA, 1% NP40, 0.7% sodium deoxycholate, 1 mM PMSF, PICs), twice in 1X TE, and eluted in elution buffer (50 mM Tris-HCl pH 8.0, 10 mM EDTA, 1% SDS). DNA samples were purified using UPrep® Spin Columns (Genesee Scientific) according to the manufacturer's instructions. PCR reactions were performed on an Applied Biosystems Step One Plus real-time PCR systems using SYBR Green PCR Master Mix in duplicate using samples from at least three independent cell harvests and the specificity of amplification was examined by melting curve analysis. The relative amounts of TOP1cc-seq DNA were quantified relative to inputs. Primers used for TOP1cc-qPCR are listed in Table S4.

For sequencing, the eluted DNA was quantified with a Qubit 4.0 fluorometer (Invitrogen), and 10 ng of DNA was used to prepare the sequencing libraries using KAPA Hyper Prep Kit (KAPA Biosystems) according to the manufacturer's instructions. Briefly, purified DNA was subjected to end-repair, adaptor ligation followed by indexed PCR. Libraries were size selected for average size of 300 bp. For GFP-FLAG-TOP1cc-seq, sequencing was performed on an Illumina® NovaSeq 6000 (Illumina, California, USA) with a read length configuration of 150 PE for 50M reads (25M in each direction) per sample.

DNA Supercoiling Assay

DNA supercoiling assays were performed based on established protocols.[90] Briefly, 12 nM of TOP1 was incubated with various amounts of refolded RNA (2-40 nM) on ice for 5 min in 1X TOP1 buffer (25 mM HEPES pH 7.6, 100 mM KCl, 0.2 mM $MgCl_2$, 0.1 mM EDTA and 10% glycerol) in a final volume of 50 μL. Following the addition of 2 nM plasmid DNA, reactions were incubated at 30°C for 10 min. The reactions were deproteinized with the addition of 12.5 μg of Proteinase K (Life Technologies) at 45°C for 10 min. Purified DNA was subjected to 0.8% agarose gel electrophoresis at 120 V for 90 min and stained with ethidium bromide for 20 min prior to imaging using LI-COR Odyssey Fc Imaging System.

Single-Molecule Magnetic Tweezer Analysis of TOP1

Single molecule magnetic tweezer experiments were performed following established protocols with a few modifications.[71] All experiments were carried out in TOP1 Dilution Buffer (10mM HEPES-KOH pH 7.6, 0.1mM EDTA pH 8.0, 10% Glycerol, 100 mM KCl) supplemented with 1mM DTT and 0.1% BSA. Recombinant TOP1 was diluted in TOP1 dilution buffer to a concentration of 1-4 nM and incubated with the *MYC* eRNA or Isoleucine tRNA from *Mycobacterium tuberculosis*.

Please cite this article in press as: Bhola et al., RNA interacts with topoisomerase I to adjust DNA topology, Molecular Cell (2024), https://doi.org/10.1016/j.molcel.2024.07.032

The DNA template used in the magnetic tweezers experiments was constructed by ligating the ends of a linearized pFOS1 plasmid with either digoxigenin or biotin functionalized ends. DNA was heated at 55°C for 5 min, then added to an equal volume of 0.6 mg/mL M270 streptavidin-coated magnetic beads across two Eppendorf tubes. The mixture was rotated at room temperature for 15 min. The flow cell was incubated with 0.1 mg/mL anti-digoxigenin antibody and 3 μm polystyrene reference beads overnight, upside down so that the beads and antibody settled onto the surface. The flow cell was prepared by running 4 to 5 flow cell volumes of 1% BSA + 1% F127 in PBS and incubating for 5 min prior to adding 10 flow cell volumes of TOP1 Dilution Buffer. The DNA/Beads mix was then added to TOP1 Dilution Buffer, and the solution was added to the flow cell. The flow cell was left upside down for a minimum of 15 min to allow the DNA to bind to antibodies on the surface.

A force calibration was conducted by varying the magnetic force on a DNA tether and monitoring the resulting extension. The position of the magnet was varied away and back towards the flow cell to determine the presence of hysteresis on the DNA. Finally, the change in linking number, denoted by the number of turns of the magnet in the experiment was monitored with DNA extension at varying forces between 0.25 and 1 pN. Following the tether calibration, a blank scan was run with TOP1 Dilution Buffer, and the magnet is turned 30 times at 0.5 pN, which match the experimental conditions after TOP1 addition. Once the scan has completed, 1 to 4 nM of recombinant TOP1 in TOP1 Dilution Buffer is added to the flow cell. Thirty positive turns are introduced into the DNA, and changes in extension because of TOP1 activity are monitored.

For experiments with RNA, a 1:1 ratio of protein:RNA is added and TOP1 activity is monitored. To confirm effects of the RNA on TOP1 activity, the flow cell was washed with Dilution Buffer prior to adding fresh TOP1 in the absence of RNA prior to a second monitoring of TOP1 activity.

QUANTIFICATION AND STATISTICAL ANALYSIS

MS Quantitative Analyses

The samples were analyzed on a nanoACQUITY UPLC-Orbit Fusion Lumos LC-MS/MS platform for 90 min. To identify the proteins associated with TOP1, we used Pandas (https://github.com/pandas-dev/pandas) in Python3 to parse the TOP1 IP-MS data according to the following parameters: common to two of the three replicates, have a $-\log_{10} p$ value $\geq$ 20, represented by $\geq$ 2 peptides, and TOP1-unique or $\geq$ 3-fold more enriched in the TOP1 relative to the IgG IP. The functional protein association networks were determined in STRING database using default parameters.[42]

ChIP-seq and TOP1cc-seq Analysis

The quality control of raw data from ChIP-seq and TOP1cc-seq was evaluated with FastQC[75] and MultiQC.[81] The low-quality reads and adapter sequences were removed using TrimGalore[84] with a phred score threshold of 30. Sequencing reads were mapped to the GRCh38 (+major SNVs) human genome using Bowtie2 v2.4.5[72] with default parameters. SAMtools v1.6.1[82] was used to filter for the mapping quality (with a MAPQ score threshold of 10) and duplicate reads were removed. For the GFP-FLAG-TOP1 WT and GFP-FLAG-TOP1 ΔRBR TOP1cc-seq experiments, the samples were also aligned to the *D. melanogaster* genome (BDGP6) for spike-in normalization. The percentage of uniquely mapped reads to *D. melanogaster* genome in each IP sample was determined and used to calculate normalization factors relative to the sample with the lowest mapping rate. The normalization factors were then used to downsample the deduplicated BAM files aligned to the human genome and only uniquely mapped reads were used for further analysis. Peak calling and broad H3K27ac and H3K4me1 regions were identified using MACS2 v2.1.1[80] and a cut-off of q<0.05 was used. For TOP1cc-seq, the enriched CDS regions in TOP1 ΔRBR as compared to TOP1 WT samples were identified using PyBigWig (github.com/deeptools/pyBigWig) by comparing the mean TOP1cc-seq signal ($\log_2$ transformed fold change over input as BPM) over the CDS for all genes. Deeptools v3.5.1[73] was used to generate normalized BigWig files, heatmap, and profile plots. Final BigWig files for each replicate were processed by calculating the $\log_2$ ratio as BPM of the IP with respect to input using "BamCompare" function in DeepTools v3.5.1.[73] The BigWig files were visualized in IGV.[79]

To identify enhancer regions in SW480 cells, we analyzed our ChIP-seq and PRO-seq data available in NCBI Gene Expression Omnibus (GEO) with the accession number GSE102796[39] and GSE20248[37] respectively. We overlapped broad ChIP-seq peaks for H3K27ac and H3K4me1 with PRO-seq peaks and removed intergenic regions found within 3.0 kb of the TSS of all annotated genes. PRO-seq peaks were called from the corresponding Bedgraph file using "bdgpeakcall" function in MACS2[80] with a minimum length threshold of 500 bp.

eCLIP Analysis

Single-end reads were trimmed using TrimGalore[84] to remove adapters and low-quality sequences (phred score threshold of 28). Reads were mapped uniquely with STAR v2.7.5[83] to the human genome (hg38). featureCounts v2.0.3[76] was used to get the read counts for eCLIP samples across all transcripts (GENCODE v45).[77] Transcripts significantly enriched for TOP1 binding were determined by analyzing the differential enrichment of TOP1 IP over IgG using DESeq2 v1.38.3.[74] The cut-off for differential enrichment was q value $\leq$ 0.05 and $\log_2$ FC $\geq$ 0.58. To identify TOP1 binding to eRNA, we overlapped the high confidence TOP1 eCLIP peaks (called using MACS3[80]) across the replicates with the unique enhancer regions in SW480 cells that were defined as described above. For generating the final BigWig files, Deeptools v3.5.1[73] was used to calculate the $\log_2$ ratio as RPKM of the TOP1 IP with respect to

the IgG IP after combining the BAM files from the two respective replicates. The gene set enrichment analysis was carried out using Enrichr.[47] Terms with an p value < 0.05 were considered statistically significant.

UV-RIP-seq and PRO-seq Analysis

The quality control of raw data was evaluated with FastQC[75] and MultiQC.[81] The UV-RIP-seq and PRO-seq reads were filtered for quality using TrimGalore.[84] Raw reads for UV-RIP-seq were mapped to the hg38 human genome using STAR v2.7.5[83] and PRO-seq reads were mapped using HISAT2 v2.2.1[78] with default parameters. PCR duplicates were removed from UV-RIP-seq data and sample-level normalization was performed using ERCC RNA Spike-in, based on the number of uniquely mapped reads to the ERCC genome across all IP samples. The final deduplicated and spike-in normalized reads were used to get the raw counts across all transcripts with featureCounts v2.0.3[76] using GENCODE v45 annotation.[77]

We identified the enriched RNAs by analyzing the differential enrichment of TOP1 IP over IgG by using DESeq2 v1.38.3.[74] The cutoff for differential enrichment was an adjusted q value $\leq$ 0.05 and a $\log_2$ FC $\geq$ 0.58 to identify the significant TOP1 associated transcripts over IgG. To identify TOP1 binding to eRNA, we overlapped the high confidence TOP1 UV-RIP-seq peaks (called using MACS3[80]) with the identified enhancer regions in SW480 cells as described above. Deeptools v3.5.1[73] was used to generate the final BigWig files by calculating $\log_2$ ratio as RPKM of the TOP1 IP with respect to IgG IP after combining BAM files from the two respective replicates. The BigWig files were visualized in IGV.[79]

To classify genes according to their expression levels, PRO-seq counts were used and to classify enhancers, PRO-seq RPKM signal at the center of the enhancer region was used. Genes and enhancers with less than 30% expression were classified as low expression, 30-90% as medium expression, and >90% high expression. Genes with zero PRO-seq counts were removed. The gene set enrichment analysis was carried out using Enrichr.[47] Terms with an p value < 0.05 were considered statistically significant. To elucidate bidirectional transcription across enhancers, the BigWig files for PRO-seq were separated and scaled into forward and reverse strands from the aligned reads using "–filterRNAstrand" parameter in Deeptools v3.5.1.[73]